Contents lists available at ScienceDirect

Journal of Energy Storage

journal homepage: www.elsevier.com/locate/est

Research Papers

A preliminary investment-screening framework for battery energy storage systems (BESS) under the uncertainty of locational marginal price (LMP) markets

Muhammad Umer [a], Kashif Imran [a,*], Waqquas Bukhsh [b], Muhammad Yousif [a]

[a] USPCAS-E, National University of Sciences and Technology (NUST), 44000, Islamabad, Pakistan
[b] Department of Electronic and Electrical Engineering, University of Strathclyde, Glasgow, G1 1XQ, UK

ARTICLE INFO

Keywords:
Variable Renewable Energy (VRE)
Locational Marginal Price (LMP)
Battery Energy Storage Systems (BESS)
Optimal investment planning
K-means clustering
Portfolio optimization
Conditional Value at Risk (CVaR)

ABSTRACT

To counter the negative impacts of Variable Renewable Energy (VRE) on grid stability and electricity pricing, Battery Energy Storage Systems (BESS) have emerged as a viable option offering grid flexibility and energy arbitrage solutions. This paper uses historical day-ahead Locational Marginal Price (LMP) data from a system operator in the United States to propose a preliminary investment-screening framework for BESS that private investors can use in any LMP market. The framework is developed in three phases and does not rely on detailed network data. In the first phase, a systematic data engineering process is conducted for four years of data on load nodes' LMPs to capture salient features of historic LMP fluctuations. Subsequently, optimal BESS investment parameters are designed, including the identification of consecutive peak and non-peak LMP values for energy arbitrage applications, as well as the evaluation of statistical indicators of average and variance to support investment planning decisions. In the second phase, the Cluster Criterion Node Selection (CCNS) and Portfolio Utility Optimization (PUO) methods are designed and utilized for the optimal siting and sizing processes, respectively. The PUO method is further divided into two distinct optimal sizing frameworks, including Mean-Variance PUO and Mean-Conditional Value at Risk (CVaR) PUO. In the final phase, a techno-economic assessment is conducted using Net Present Value (NPV) and Internal Rate of Return (IRR) to evaluate the financial viability of Lithium-Ferro-Phosphate-Lithium-ion (LFP) and Vanadium Redox Flow (Vd) technologies under two base scenarios and sensitivity analyses, incorporating degradation models, replacement schedules, and tax credit mechanisms. Results show that, using the Mean-CVaR PUO model under the "With Investment Tax Credit (ITC)" scenario, the highest returns were achieved by LFP technology in 2033, with an NPV of approximately USD 24.3 Million and an IRR of 18%. These findings support the viability of both LFP and Vd BESS investment options, with proposed research providing a preliminary investment-screening decision-making tool for private investors who lack access to detailed grid data, such as network topology or impedance characteristics, flows, and capacities of transmission lines.

Abbreviations

BESS	Battery Energy Storage Systems.	PD	Project Development.
CCNS	Cluster Criterion Node Selection.	PE	Power Equipment.
DR	Discount Rate.	RTE	Round Trip Efficiency.
EPC	Engineering Procurement & Construction	ITC	Investment Tax Credit.
CC	Control & Communication.	IRA	Inflation Reduction Act.
GI	Grid Integration.	IRR	Internal Rate of Return.

(*continued on next column*)

(*continued*)

LFP	Lithium-Ferro-Phosphate-Lithium-ion.	INVF	Individual Node Value Function.
LMP	Locational Marginal Price.	SB	Storage Block.
MILP	Mixed Integer Linear Programming.	SBOS	Storage Balance of System.
MISO	Midcontinent Independent System Operator.	SI	System Integration.
NPV	Net Present Value.	Vd	Vanadium Redox Flow.

(*continued on next page*)

* Corresponding author.
E-mail address: kashifimran@uspcase.nust.edu.pk (K. Imran).

https://doi.org/10.1016/j.est.2026.123883
Received 31 December 2025; Received in revised form 12 June 2026; Accepted 24 July 2026

(*continued*)

PUO	Portfolio Utility Optimization.	VRE	Variable Renewable Energy.
CVaR	Conditional Value at Risk	VaR	Value at Risk
Co-CVaR	Co-Conditional Value at Risk		

Parameters, symbols, and notations

$P_n^{con,avg}$	Average of the consecutive peak LMP values for the n^{th} node.
$NP_n^{con,avg}$	Average of the consecutive non-peak LMP values for the n^{th} node.
DDL_n	Delta Daily LMP for the n^{th} node.
Z_n	Zeta, representing the return from charging and discharging a BESS deployed at the n^{th} node.
$E_{discharge}$	Energy discharged from the BESS during the peak hours for selling at a higher LMP.
E_{charge}	Energy charged into the BESS during off-peak hours for purchasing at a lower LMP.
$T_{ch/di}$	Number of charging/ discharging hours for batteries.
Z_n^{avg}	Average of Z_n values over all hours of days in Y years for the n^{th} node.
Z_n^{var}	Variance of Z_n values over all hours of days in Y years for the n^{th} node.
Z_n^{diff}	Daily percentage Zeta difference.
t	Day in daily Z_n^{diff} observations ($t = 2, 3, \ldots, T$).
$tail_n$	Set of the worst τ observations for the n^{th} node.
τ	Number of worst observations in the $tail_n$ for the n^{th} node.
z	Individual Z_n^{diff} observations contained in tail_n.
$Z_{n,t}$	Zeta value at node n on day t.
T	Total number of daily Z_n^{diff} observations of the n^{th} node across all Y years.
$Z_n^{VaR(95\%)}$	Value of Risk for the n^{th} node at 95% confidence level.
$Z_n^{CVaR(95\%)}$	Conditional Value of Risk for the n^{th} node at 95% confidence level.
$Z_m^{CVaR(95\%)}$	Conditional Value of Risk for the m^{th} node at 95% confidence level.
$Z_p^{CVaR(95\%)}$	Conditional Value of Risk for the p^{th} node at 95% confidence level.
$Z_{n\|n''}^{Co-CVaR(95\%)}$	Conditional expectation of node n given that node n'' is experiencing its worst outcomes at 95% confidence level.
$Z_{n''\|n}^{Co-CVaR(95\%)}$	Reverse conditional expectation of node n given that node n'' is experiencing its worst outcomes at 95% confidence level.
$Z_{n,n''}^{Co-CVaR(95\%)}$	Symmetric Co-CVaR, defined as the average of conditional and reverse conditional expectations between two nodes n and n''
$Z_{p,p''}^{Co-CVaR(95\%)}$	Symmetric Co-CVaR, defined as the average of conditional and reverse conditional expectations between two nodes p and p''
Z_p^{avg}	Average of Z_n values over all hours of days in Y years for the p^{th} node.
Z_p^{var}	Variance of Z_n values over all hours of days in Y years for the p^{th} node.
Z_m^{avg}	Average of Z_n values over all hours of days in Y years for the m^{th} node.
Z_m^{var}	Variance of Z_n values over all hours of days in Y years for the m^{th} node.
$Z_{n,y,d,h}$	Z_n value in year y, day d, and hour h for the n^{th} node.
$Z_{n,n'}^{covar}$	Covariance in Z_n values between two nodes n and n' or all hours of days in Y year.
$Z_{p,p'}^{covar}$	Covariance in Z_n values between two nodes p and p' or all hours of days in Y year.
DoD	Depth of discharge in %.
$BESS_{MWh}^{Total}$	BESS energy rating for total investment in MWh.
$BESS_{MW}^{Total}$	BESS power rating for total investment in MWh.
$BESS_{MWh}^{DoD}$	BESS energy rating for total investment based on depth of discharge in MWh.
$BESS_{MWh}^{DoD_p}$	BESS energy rating for the p^{th} node based on depth of discharge in MWh.
$BESS_{MWh}^{p}$	BESS energy rating for the p^{th} node investment in MWh.
$BESS_{MW}^{p}$	BESS power rating for the p^{th} node investment in MW.
$Z_n^{avg,norm}$	Normalized value of Z_n^{avg}.
$Z_n^{var,norm}$	Normalized value of Z_n^{var}.
x_n	Two-dimensional feature vector input for k-means clustering.
$\|C_i\|$	Total count of nodes in cluster i.
C_i	Set of nodes assigned to cluster i.
μ_i	Centroid of each cluster i.
Z_k^{avg}	Average of $Z_n^{avg,norm}$ values for all nodes in the k^{th} cluster.
Z_k^{var}	Average of $Z_n^{var,norm}$ values for all nodes in the k^{th} cluster.
N_k	Total number of nodes within the k^{th} cluster.
C_k	Cluster Score for k^{th} cluster.
C_{opt}	Optimal Cluster Score.
$INVF_m$	INVF for the m^{th} node.

(*continued on next column*)

(*continued*)

$INVF_p$	INVF for the p^{th} node.
A_{risk}	Mean-Variance Risk aversion factor.
λ	Mean-CVaR Risk aversion coefficient.
U_g	Mean-Variance Portfolio Utility Function.
U_g'	Mean-CVaR Portfolio Utility Function.
x_p	Mean-Variance Portfolio weights for each of the top 'p' optimal node.
x_p'	Mean-CVaR Portfolio weights for each of the top 'p' optimal node.
$x_{p''}'$	Mean-CVaR Portfolio weights for each of the top 'p''' optimal node.
$SB_{\$/MWh}$	Storage Block Cost in \$/MWh for the b^{th} BESS technology.
$SBOS_{\$/MWh}$	Storage Balance of System Cost in \$/MWh for the b^{th} BESS technology.
$SI_{\$/MWh}$	System Integration Cost in \$/MWh for the b^{th} BESS technology.
$EPC_{\$/MWh}$	Engineering Procurement & Construction Cost in \$/MWh for the b^{th} BESS technology.
$PD_{\$/MWh}$	Project Development Cost in \$/MWh for the b^{th} BESS technology.
$V_{O\&M}^{\$/MWh}$	Variable operational and maintenance in \$/MWh for the b^{th} BESS technology.
$RTE_{losses}^{\$/MWh}$	RTE losses in \$/MWh for the b^{th} BESS technology.
$RTE_{loss}(\$)$	RTE losses in \$ for the b^{th} BESS technology for the b^{th} BESS technology.
$V_{O\&M}(\$)$	Variable operational and maintenance in \$ for the b^{th} BESS technology.
$PE_{\$/MW}$	Power Equipment Cost in \$/MW for the b^{th} BESS technology.
$CC_{\$/MW}$	Control & Communication Cost in \$/MW for the b^{th} BESS technology.
$GI_{\$/MW}$	Grid Integration Cost in \$/MW for the b^{th} BESS technology.
$I_{\$/MWh}$	Total Installation Cost in \$/MWh for the b^{th} BESS technology.
$I_{\$/MW}$	Total Installation Cost in \$/MW for the b^{th} BESS technology.
$F_{O\&M}^{\$/MW-yr}$	Fixed operational and maintenance in \$/MW-yr for the b^{th} BESS technology.
$F_{O\&M}(\$)$	Fixed operational and maintenance in \$ for the b^{th} BESS technology.
N_b^{rep}	Total number of storage block replacements of b^{th} BESS technology.
Y_{max}^{lc}	The longest life cycle among all BESS technologies.
Y_b^{lc}	Useful life or duration corresponding to life cycle of b^{th} BESS technology in years.
S_{BR}	Set of storage block replacement years for the p^{th} node.
$Q_{cyc,b}^{daily}$	Daily cyclic loss rate in % for the b^{th} BESS technology.
$Q_{cal,b}^{annual}$	Calendar loss in % for the b^{th} BESS technology.
$C_{p,b}^{Opr}$	Total annual operation cost in \$ over the useful life of storage block for the p^{th} node and the b^{th} BESS technology.
$C_{p,b}^{Ins}$	Total initial installation cost in \$ for pth node and the b^{th} BESS technology.
$C_{p,b}^{Rep}$	Replacement cost for the p^{th} node and the b^{th} BESS technology.
$C_{p,b}^{Sal}$	Salvage cost for the p^{th} node and the b^{th} BESS technology.
$R_{p,b}^{y}$	Annual net arbitrage revenue in \$ for the p^{th} node and the b^{th} BESS technology based on the degradation of SB.
$CF_{p,b}^{y}$	Annual net cash flows for p^{th} node and the b^{th} BESS technology in \$.
$NPV_{p,b}$	NPV for p^{th} node and the b^{th} BESS technology is calculated in \$.
$NPV_{P_{nodes},b}$	Total NPV for all P_{nodes} nodes and the b^{th} BESS technology is calculated in \$.
DR	Discount Rate.
$CF_{P_{nodes},b}^{y}$	Annual net cash flow for all P_{nodes} nodes and the b^{th} BESS technology in \$.
$C_{P_{nodes},b}^{Ins}$	Total initial installation cost in \$ for all P_{nodes} nodes and the b^{th} BESS technology in \$.
$C_{P_{nodes},b}^{Rep}$	Net replacement cost for all P_{nodes} nodes and the b^{th} BESS technology in \$.
$C_{P_{nodes},b}^{Sal}$	Salvage cost of SB for all P_{nodes} nodes and the b^{th} BESS technology in \$.
$IRR_{P_{nodes},b}$	Net IRR for all P_{nodes} nodes and the b^{th} BESS technology.
Y	Total number of years.
D	Total number of days in a year.
h	Number of hours in a day.
h_w	Consecutive hour index within the 4-hour block.
h_s	Consecutive starting hour index within the 4-hour block.
LMP_{n,h_w}	LMP at the n^{th} node and h_w^{th} hour.
r	Replacement index for the b^{th} BESS technology.
y_r	The year in which a storage block replacement occurs.
b	Index representing the b^{th} technology.
γ_y	Calendar loss factor for 'y' year.
n	Index representing the n^{th} node.

(*continued on next page*)

(*continued*)

n'	Index representing a secondary or comparative node with the primary the n^{th} node, used for calculating covariance.
n''	Index representing a secondary or comparative node with the primary the n^{th} node, used for calculating tail co-risk in Mean-CVaR PUO.
i	Index of the i^{th} cluster in the k-means clustering algorithm.
m	Index of the m^{th} optimal node $(m \in C_{opt})$.
k_{elbow}	Optimal number of clusters selected by elbow method.
$k_{silhouette}$	Optimal number of clusters selected by silhouette method.
k	Optimal number of clusters based on the average of the numbers selected by the elbow and silhouette methods.
p	Index of the top p^{th} optimal node.
p'	Index representing a comparative node with the primary p^{th} node, used in portfolio optimization.
p''	Index representing a secondary or comparative node with the primary p^{th} node, used for calculating tail co-risk in Mean-CVaR PUO.
N_{nodes}	Total number of nodes indexed by 'n'.
M_{nodes}	Total number of optimal nodes indexed by 'm'.
P_{nodes}	Total number of top selected optimal nodes indexed by 'p'.
$K_{clusters}$	Total number of clusters, indexed by 'k'
B_{Total}	Total number of BESS technologies indexed by 'b'.

1. Introduction

In recent years, the global energy landscape has undergone significant transformation with the increasing integration of Variable Renewable Energy (VRE) sources, such as wind and solar, to meet climate change targets. While VRE adoption is crucial for decarbonization, its inherent intermittency introduces challenges in maintaining power system stability, particularly with the growing electrification of heating, transportation, and industrial processes. These fluctuations in supply and demand need enhanced grid flexibility, often achieved through fast-ramping generation and quick-start capabilities [1]. Energy Storage Systems have emerged as a pivotal solution to mitigate these challenges, ensuring grid reliability and efficiency. Among various energy storage systems technologies, Battery Energy Storage Systems (BESS) have gained prominence due to their high power and energy density, rapid deployment, and ability to provide instantaneous grid support [2]. Enhancing grid stability, deferring infrastructure upgrades, and improving transmission congestion are further contributions of BESS to improve operational efficiency and cost savings at the utility-scale [3].

Utility-scale BESS can be deployed either as standalone units or integrated into hybrid VRE-storage systems. Their multifunctional capabilities enable participation in electricity markets through energy arbitrage, frequency regulation, voltage support, black-start services, and mitigation of VRE forecast errors [4]. This versatility makes BESS a critical asset in modern, decentralized power systems, improving reliability and power quality during higher renewable penetration. BESS operators, whether utilities or private investors, can maximize their economic returns by strategic participation in day-ahead, real-time, and ancillary service markets. Effective revenue optimization hinges on sophisticated scheduling models, particularly in competitive LMP-based markets [5]. Among available services, energy arbitrage remains one of the most lucrative because it allows storage owners to capitalize on temporal price differentials by charging during low-price periods and discharging during peak demand. This load-shifting capability not only enhances demand-side management but also improves the economic viability of BESS investments [6]. However, realizing these benefits depends on optimal investment decisions, the LMP-based BESS placement strategy is crucial for maximizing arbitrage profits and ensuring long-term economic feasibility [2]. Consequently, effective BESS investment planning must incorporate both optimal location selection and capacity determination to enhance profitability while supporting grid stability [7].

This paper addresses the challenges of price volatility in LMP markets and the limited availability of detailed network data during BESS investment planning for private investors. It proposes an initial preliminary investment screening tool relying on an LMP-based framework for the siting and sizing of BESS, in contrast to conventional methods that require extensive grid information such as voltage, phase angle, active and reactive power flows, contingencies, and outage data. Since LMP inherently represents a combination of energy cost, congestion cost, and loss components, it can serve as a comprehensive indicator for decision-making without the need for detailed network parameters. Furthermore, the LMP based data-driven approach is robust because of the very reason that LMPs capture underlying network power flow conditions. Therefore, the LMP based data-driven approach is a viable alternative to full network power flow analysis, especially if technical data of grid is not available. The proposed planning approach spreads over three distinct phases. The first phase involves collecting the historical day-ahead LMP data from the website of the Midcontinent Independent System Operator (MISO) of the United States. Data analytics of hourly LMP load nodes over the past four years (calendar years 2021–2024) are used to identify temporal trends and volatility patterns, enabling the development of an energy arbitrage model that incorporates consecutive peak and off-peak LMP blocks for optimal BESS charging and discharging scheduling. Further, BESS optimal investment parameters are designed based on two key statistical indicators of average and variance, which are used to identify LMP nodes that maximize returns (high average LMP) while simultaneously minimizing risk (low LMP variance). In the second phase, two distinct methodologies, Cluster Criterion Node Selection (CCNS) and Portfolio Utility Optimization (PUO), are implemented for optimal siting and sizing and tested on two predominant BESS technologies. The CCNS clusters LMP nodes and ranks them in order of preferred BESS sites based on selected statistical parameters (average and variance) through the Individual Node Value Function (INVF). Next, PUO utilizes Markowitz's portfolio optimization to allocate optimal capacity shares among the top selected nodes for initial assessment. This optimization-based approach is extended with two risk frameworks. Mean-Variance PUO uses covariance to capture overall return co-movements, while Mean-CVaR PUO replaces variance with Conditional Value at Risk (CVaR) and Co-Conditional Value at Risk (Co-CVaR). CVaR measures the expected loss during the worst 5% of market days, capturing downside tail risk that variance overlooks, while Co-CVaR quantifies how nodes behave simultaneously during extreme events, capturing tail dependence between the candidate nodes. These tail-risk measures are particularly valuable for BESS investors concerned with protecting against large losses during market stress. In the final phase, a techno-economic assessment is conducted using Net Present Value (NPV) and Internal Rate of Return (IRR) to evaluate the financial viability of Lithium-Ferro-Phosphate-Lithium-ion (LFP) and Vanadium Redox Battery (Vd) technologies under two base scenarios and sensitivity analyses, incorporating degradation models, replacement schedules, and tax credit frameworks. The notable contributions of this paper are summarized as follows:

- Developing an energy arbitrage model to determine consecutive peak and non-peak LMP blocks for BESS discharging and charging, respectively.
- Designing robust preliminary optimal investment parameters for BESS under uncertainty without using the detailed grid network data.
- Identifying the most feasible LMP nodes for optimal siting and sizing of BESS by using CCNS and PUO.
- Performing a comprehensive scenario-wise techno-economic assessment across two predominant BESS technologies and determining the most economically viable BESS technology for optimal deployment.

The rest of the paper is structured as follows. Section 2 presents a literature review covering recent developments in BESS investment planning and highlighting the existing gaps. Section 3 outlines the proposed methodology, which is structured into three sequential phases. Section 4 elaborates on the outcomes and results, while Section 5 provides the conclusion and identifies possible ways in which this work can be extended in the future.

2. Literature review

This section reviews global research contributions on methodologies for optimizing BESS scheduling, placement, and capacity determination, emphasizing their role in enhancing cost-effectiveness, efficiency, and resilience in energy systems. The authors in [8] proposed an optimal LMP-based scheduling mechanism for grid-connected microgrids by using BESS and renewable energy resources integration. Similarly, [9] developed a dynamic optimal power flow model for grid-scale BESS scheduling with minimal generation costs and balancing between electricity supply and demand. Following this, a mean-variance optimization model is proposed by [5] for energy storage scheduling to balance risk and revenue under day-ahead and real-time LMP uncertainties.

In parallel with optimal scheduling and operational optimization efforts, the interplay between BESS and VREs has been extensively studied. The authors of [10] proposed optimal placement and capacity distribution of the BESS in a solar PV integrated network, significantly reducing curtailments. Moreover, [7] investigated BESS allocation in high wind-penetration systems, to enhance the functional capabilities and stability of power transmission systems. For large-scale renewable integration, [11,12] presented a mixed-integer linear programming (MILP) approach for BESS integration to support a highly renewable-penetrated unbalanced distribution network by determining the optimal sizes and locations for BESS. To analyze the role of effective BESS operational planning in distribution networks, the author in [2] examined the role of optimal siting and sizing of BESS operations to significantly reduce transmission congestion and electricity price volatility through Bayesian optimization and a congestion-based heuristic framework. Multi-objective optimization models for the optimal placement and capacity sizing of BESS in the distribution network are formulated in [13,14], focusing on effectively reducing overall system costs, power losses, and voltage deviations.

BESS has been deployed to enhance overall stability and reliability in transmission grids dominated by VREs. The methodology discussed by [15] integrates active power frequency sensitivity analysis with reactive power limit evaluation to identify the most effective bus for BESS siting and sizing while balancing frequency support with voltage stability constraints. To improve transient voltage and frequency stability in weak grids, [16] utilized the Adaptive Grey Wolf Optimization algorithm for optimal allocation and capacity sizing of BESS. Moreover, recent research trends indicate a shift toward more integrated optimization frameworks. The authors of [17] have demonstrated a strategic tri-level optimization framework for siting and sizing of BESS to reduce grid vulnerability, improve voltage stability, enhance frequency regulation, and facilitate better peak shaving. Similarly, the authors of [18] formulated mixed-integer linear programming to optimize the integration of energy storage systems within a transmission network, specifically focusing on the co-optimization of storage sizing, placement, and transmission line constraints to minimize total investment and operational costs. Building on this optimization perspective, another study [19] proposed a multi-phase BESS optimal sizing framework that employs the *Z*-bus matrix for sensitivity analysis to iteratively narrow the search space for optimal BESS capacities at selected locations, for maximizing system reliability as well as net benefits of both system operators and private investors.

To analyze the BESS techno-economic investment potential, the study by [20] have explored the integration of BESS with existing photovoltaic systems, considering various market types and ownership models using the MILP model. Extending this MILP framework for ownership modeling, the subsequent study by [1] highlights that integrating demand response with BESS in LMP-based markets enhances operational flexibility and economic efficiency for system operators. Furthermore, BESS profitability in electricity markets has been explored through a diverse range of optimization frameworks. The study by [4] introduced a novel optimization technique for long-term BESS planning in wholesale markets, ensuring profitability without external financial support. Comparative analysis of optimization techniques is conducted in [21] to evaluate linear programming, MILP, and mixed-integer nonlinear programming to ensure the highest net cumulative profit for energy arbitrage during price fluctuations of a grid-integrated BESS. Similarly, [22] has analyzed two models for optimal investment timing and sizing for the Irish electrical grid, allowing private investors to purchase BESS capacity based on anticipated costs. To analyze the role of BESS in energy market risks, [23] introduced an optimal BESS capacity sizing framework to mitigate strategic collusion in the electricity day-ahead market, enhancing competitiveness without policy interventions. To improve and quantify price-quantity bidding, [6] employed a stochastic Monte Carlo simulation-based BESS bidding model for day-ahead and real-time energy markets. While investigating the BESS participation in electricity markets and demand side management under uncertainty, the study in [24] utilized a distributionally robust optimization method to solve the mean-risk portfolio optimization, employing the Value-at-Risk index.

To rigorously quantify tail-risk exposures, the Conditional Value-at-Risk (CVaR) has been extensively adopted across both long-term investment planning and real-time operational control of BESS. For strategic planning, [43] incorporated CVaR into a multi-level BESS sizing model to manage financial risks under market price and capacity uncertainties, while [44] employed CVaR within a two-stage integrated energy system planning framework to optimally trade off capital costs against potential operational risk losses. On the operational front, [45] formulated a rolling-horizon linear programming approach that minimizes the CVaR of battery operating costs, effectively buffering grid-connected microgrids against short-term demand and electricity price volatilities.

In recent studies, the Markowitz portfolio optimization theory has achieved a balanced risk-return trade-off in investment planning for the power sector. The authors of [25] developed a Markowitz portfolio optimization-based matchmaking algorithm for load serving entities to maximize expected utility while improving power allocation to bilateral trading options under market uncertainty. Moreover, the optimized electricity retailer portfolios were developed by [26] within a multi-agent system, utilizing Markowitz portfolio theory, to manage risk and maximize returns by selecting optimal end-consumer groups. While developing a framework for end-user flexibility within day-ahead and intraday markets, [27] utilized a rolling horizon approach and Markowitz portfolio optimization to reduce costs within a dynamic market context. To optimize the geographical allocations of renewable energy sources, the study by [28] applied the Markowitz Theory with temporal correlations to reduce power system balancing needs and uncertainty. Similarly, the study by [29] evaluated the integration of wind power into Colombia's hydro-dominated energy system using Markowitz portfolio theory, combined with machine learning techniques, to optimize overall risk and return.

Several studies have demonstrated the role of artificial intelligence and advanced data analytics in optimal BESS management, load forecasting, and optimal siting and sizing applications. The authors of [30] introduced an optimized energy management framework for grid-connected microgrids, using k-means clustering and artificial neural networks for load forecasting. [31] proposed an artificial intelligence-based genetic algorithm to optimize the allocation of BESS, electric vehicle charging stations, and distributed generation units in distribution networks. Furthermore, to analyze the potential of optimal siting and sizing of BESS, [32] proposed optimal BESS placement in VRE-integrated systems by using k-means for clustering historical substation load profiles data, enabling the deferral of distribution network upgrades and providing economic benefits assessed through NPV analysis. Similarly, [33] utilized the Distribution Locational Marginal Pricing in a bilevel stochastic programming model for optimal siting and sizing of BESS in distribution systems, along with k-means clustering to generate various operating scenarios, highlighting its role in incentivizing BESS investments through dynamic price signals.

3. Methodology

This section details the methodological steps undertaken to optimize the BESS siting and sizing process by using publicly available data of day-ahead LMPs in the MISO system for four years, from 2021 to 2024 [34]. The LMP data of load nodes is selected because this study explores BESS deployment at load nodes. The overall methodology is divided into the following three phases:

- **Phase-I:** Designing a preliminary optimal BESS investment parameters, incorporating an energy arbitrage model for BESS charging and discharging time periods.
- **Phase-II:** Optimal selection of nodes for BESS siting and sizing, which is done through CCNS and PUO methods, respectively.
- **Phase-III:** Optimal BESS technology selection through scenario-wise techno-economic assessment of two BESS technologies by NPV and IRR.

Further details of all the respective phases of the methodology are explained in the following subsections.

3.1. Designing optimal BESS investment parameters

This phase of the paper provides the foundation of the optimal BESS siting, sizing, and technology selection process. The detailed steps for developing the energy arbitrage model based on consecutive peak and off-peak LMP blocks, statistical parameters (average, variance, and covariance), and BESS energy and power ratings are presented in the subsequent sections, ensuring realistic BESS operation.

3.1.1. Calculating consecutive optimal peak and non-peak LMP averages

In anticipating energy arbitrage with BESS, determining the consecutive charging and discharging hours' blocks is crucial. For this purpose, the concept of consecutive 4-h block averages is used in this paper to recognize that BESS typically operates over extended consecutive periods rather than isolated optimal hours.

The LMP values over a 24-h horizon are analyzed using a 4-h rolling horizon planning process, as discussed earlier in [27] to establish the most and least expensive consecutive periods for electricity transactions. This 4-h duration is selected based on industry trends, as it has historically captured most of the electricity market for storage services, as discussed in [35]. The consecutive peak LMP average for the n^{th} node is defined as the 4-h block with the highest average LMP value, making this period strategically important for discharging the BESS during peak demand periods and as represented in (1).

$$\mathrm{P}_{\mathrm{n}}^{\mathrm{con,avg}} = \left\{ \max_{\mathrm{h_w} \in \left\{1,2,\ldots,24-\mathrm{T_{ch/di}}+1\right\}} \left(\frac{1}{\mathrm{T_{ch/di}}} \sum_{\mathrm{h_w}=\mathrm{h_s}}^{\mathrm{h_s}+\mathrm{T_{ch/di}}-1} \mathrm{LMP_{n,h_w}} \right) \middle| \left(\frac{1}{\mathrm{T_{ch/di}}} \sum_{\mathrm{h_w}=\mathrm{h_s}}^{\mathrm{h_s}+\mathrm{T_{ch/di}}-1} \mathrm{LMP_{n,h_w}} \right) \neq 0 \right\} \tag{1}$$

where, n represents the node index representing the LMP of the n^{th} node, h_s represents the consecutive starting hour index within the 4-h block, h_w represents the consecutive hour index within the 4-h block, $T_{ch/di}$ represents the number of charging/discharging hours for batteries ($T_{ch/di} = 4$), LMP_{n,h_w} represents the LMP at node n and hour h_w. However, $P_n^{con,avg}$ represents the consecutive peak LMP average for the n^{th} node. Similarly, hours of the four lowest LMP values are defined as the consecutive non-peak LMP average for the n^{th} node, making these hours strategically important for charging the BESS during non-peak periods, is denoted as $NP_n^{con,avg}$ and represented in (2).

$$NP_n^{con,avg} = \left\{ \min_{h_w \in \left\{1,2,\ldots,24-T_{ch/di}+1\right\}} \left(\frac{1}{T_{ch/di}} \sum_{h_w=h_s}^{h_s+T_{ch/di}-1} LMP_{n,h_w} \right) \middle| \left(\frac{1}{T_{ch/di}} \sum_{h_w=h_s}^{h_s+T_{ch/di}-1} LMP_{n,h_w} \right) \neq 0 \right\} \tag{2}$$

3.1.2. Daily delta LMP calculations

The difference between the average optimal peak and non-peak hours is defined as the daily delta LMP, denoted as DDL_n for the n^{th} node and represented by:

$$DDL_n = P_n^{con,avg} - NP_n^{con,avg} \tag{3}$$

Moreover, DDL_n is a crucial parameter for quantifying the daily price spread in the electricity market that indicates the potential profitability of energy arbitrage using a BESS at the n^{th} node.

3.1.3. Calculation of investment return (zeta)

In BESS investment planning for selecting optimal deployment locations, a utility function can assess and optimize the decision-making process by weighing the potential returns against the anticipated risks for each candidate location based on data analytics of LMP values at deployment nodes. An investor in BESS will prefer certain energy arbitrage opportunities based on the expected returns derived from differences in consecutive peak and off-peak LMP values. For this purpose, the concept of return is generically defined by (4):

$$return = \frac{revenue - cost}{cost} \tag{4}$$

LMP and consequent returns of BESS investments are both stochastic random variables, requiring statistical data analytics for optimal BESS investment planning. The stochastic random variable of return on investment is termed Zeta for this research work. Using (4), the specific return or Zeta for BESS deployment at the n^{th} node is calculated as:

$$Z_n = \frac{\left(E_{discharge} \times P_n^{con,avg}\right) - \left(E_{charge} \times NP_n^{con,avg}\right)}{E_{charge} \times NP_n^{con,avg}} \tag{5}$$

where Z_n is denoted as Zeta, representing the return from charging and discharging a BESS deployed at the n^{th} node, $E_{discharge}$ represents the energy discharged (MWh) from the BESS during the peak hours for selling at a higher LMP and E_{charge} represents the energy charged (MWh) into the BESS during off-peak hours for purchasing at a lower LMP. While assuming no losses, BESS operates with 100% efficiency, and the discharged energy equals the charged energy ($E_{charge} = E_{discharge}$). Consequently, (5) becomes:

$$Z_n = \frac{P_n^{con,avg} - NP_n^{con,avg}}{NP_n^{con,avg}} \tag{6}$$

Now, by substituting (3) in (6), the final expression for Z_n is represented as:

$$Z_n = \frac{DDL_n}{NP_n^{con,avg}} \tag{7}$$

3.1.4. Calculating average, variance and covariance of zeta

Identifying nodes that maximize returns (high average delta LMP) while simultaneously minimizing risk (low delta LMP variance) helps to optimize BESS siting and sizing decisions. For this purpose, the daily average and variance of Z_n for the n^{th} node are mathematically represented as:

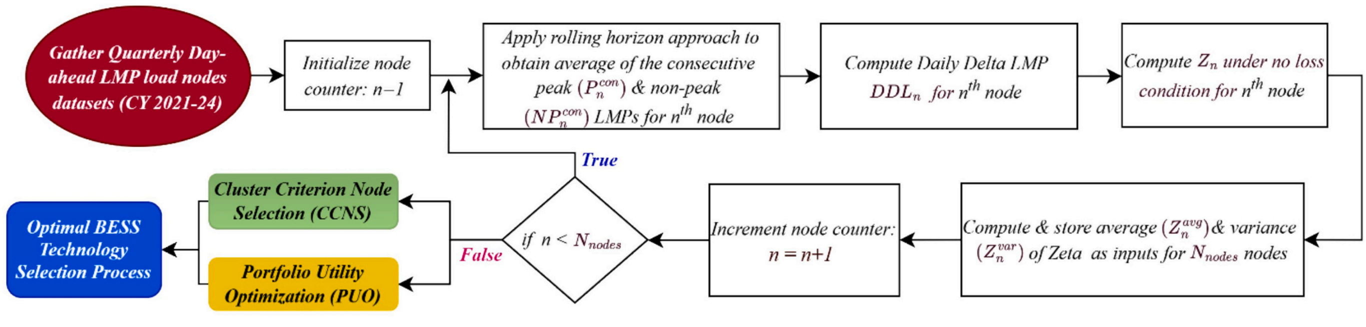

Fig. 1. Optimal BESS investment design parameters.

$$Z_n^{avg} = \frac{1}{Y \times D \times 24} \sum_{y=1}^{Y} \sum_{d=1}^{D} \sum_{h=1}^{24} Z_{n,y,d,h} \tag{8}$$

$$Z_n^{var} = \frac{1}{(Y \times D \times 24) - 1} \sum_{y=1}^{Y} \sum_{d=1}^{D} \sum_{h=1}^{24} \left(Z_{n,y,d,h} - Z_n^{avg}\right)^2 \tag{9}$$

$$Z_{n,n'}^{covar} = \frac{1}{(Y \times D \times 24) - 1} \sum_{y=1}^{Y} \sum_{d=1}^{D} \sum_{h=1}^{24} \left(Z_{n,y,d,h} - Z_n^{avg}\right) \times \left(Z_{n',y,d,h} - Z_{n'}^{avg}\right) \tag{10}$$

where, Z_n^{avg}represents the average of Z_n values over all hours of days in Y years for the n^{th} node, Z_n^{var}represents the variance of Z_n values over all hours of days in Y years for the n^{th} node, Y is the total number of years, D is the total number of days in a year, $Z_{n,y,d,h}$ represents the Z_n value in year y, day d, and hour h for the n^{th} node, $Z_{n,n'}^{covar}$represents the covariance in Z_n values between two nodes n and n' for all hours of days in Y year and n' represents the index for the secondary or comparative node with the primary n^{th} node, used for calculating covariance.

3.1.5. *Calculating value at risk, conditional value at risk and co-conditional value at risk of zeta*

For BESS investment decisions, investors are primarily concerned with downside tail risk scenarios where returns are exceptionally low or negative during extreme market conditions. Therefore, the Value at Risk (VaR), Conditional Value at Risk (CVaR), and Co-Conditional Value at Risk (Co-CVaR) act as complementary risk measures that focus exclusively on the worst-case outcomes of Zeta. Before calculating tail risk measures, the daily percentage Zeta difference is calculated for BESS investment for the n^{th} node. Unlike the hourly Zeta values defined in (7), which represent returns for individual hours, the daily percentage Zeta difference captures the day-over-day change in investment performance and calculated as:

$$\mathrm{Z}_{\mathrm{n}}^{\mathrm{diff}} = -\frac{\mathrm{Z}_{\mathrm{n,t}} - \mathrm{Z}_{\mathrm{n,t-1}}}{100}, \mathrm{t} = 2, 3, \ldots, \mathrm{T} \tag{11}$$

where Z_n^{diff} is the daily percentage Zeta difference, $Z_{n,t}$ represents the Zeta value at node n on day t, and T is the total number of daily Z_n^{diff}observations of the n^{th} node across all Y years. The negative sign converts a decrease in Zeta (adverse movement) into a positive Z_n^{diff} value, and an increase in Zeta (favorable movement) into a negative Z_n^{diff} value. Thus, higher positive Z_n^{diff} values indicate greater tail risk.

Let $Z_{n,(1)}^{diff} \leq Z_{n,(2)}^{diff} \leq \cdots \leq Z_{n,(T)}^{diff}$ represent the $Z_n^{diff}$for the n^{th} node sorted in ascending order. For a 95% confidence level, the $tail_n$ is defined as the set of the worst τ observations for the n^{th} node:

$$\mathrm{tail}_{\mathrm{n}} = \left\{ \mathrm{Z}_{\mathrm{n,(T-\tau+1)}}^{\mathrm{diff}}, \mathrm{Z}_{\mathrm{n,(T-\tau+2)}}^{\mathrm{diff}}, \ldots, \mathrm{Z}_{\mathrm{n,(T)}}^{\mathrm{diff}} \right\} \tag{12}$$

where $\tau = \lceil 5\% \times T \rceil$ is the number of worst observations in the $tail_n$ for the n^{th} node. Next VaR is calculated, which is a statistical measure that quantifies the return threshold below which a given percentage of observations fall. In this study, Zeta VaR is defined at the 95% confidence level as the threshold that separates the worst 5% of $Z_{n,t}^{\mathrm{diff}}$ from the remaining 95%. Using the tail definition from (12), Zeta VaR for the n^{th} node is defined as:

$$Z_n^{VaR(95\%)} = min(tail_n) \tag{13}$$

Where $Z_n^{VaR(95\%)}$ is the Zeta VaR and represents the smallest value in the tail set for the n^{th} node. $Z_n^{VaR(95\%)}$ indicates the threshold for extreme events, it does not provide information about the magnitude of losses beyond that threshold. Therefore, CVaR addresses this limitation by calculating the average return during extreme events. By using the tail definition from (12), Zeta CVaR at 95% confidence level for the n^{th} node is defined as the average of the τ observations in tail$_n$:

$$Z_n^{CVaR(95\%)} = \frac{1}{\tau} \sum_{z \in tail_n} z \tag{14}$$

where, $Z_n^{CVaR(95\%)}$ represents the Zeta CVaR and z represents each Z_n^{diff}observations contained in tail$_n$. Since, $Z_n^{CVaR(95\%)}$ measures the standalone tail risk of individual nodes, it does not capture how nodes behave simultaneously during extreme market conditions. Therefore, Zeta Co-CVaR $\left(Z_{n,n''}^{Co-CVaR(95\%)}\right)$ at 95% confidence level is introduced to measure tail dependence between two BESS deployment nodes. It measures the tail dependence between two nodes n and n'' for all trading days across Y years, where node n is the node whose conditional tail risk is being evaluated, while node n'' is the secondary or comparative node with the primary n^{th} node, used for calculating tail co-risk. For that purpose, the conditional expectation ($Z_{n|n''}^{Co-CVaR(95\%)}$) is first calculated as:

$$\mathrm{Z}_{\mathrm{n|n''}}^{\mathrm{Co-CVaR(95\%)}} = \frac{1}{\tau} \sum_{t \in \mathrm{tail}_{n''}} Z_{n,t}^{diff} \tag{15}$$

Similarly, the reverse conditional expectation $Z_{n''|n}^{Co-CVaR(95\%)}$ is calculated as:

$$Z_{n''|n}^{Co-CVaR(95\%)} = \frac{1}{\tau} \sum_{t \in tail_n} Z_{n'',t}^{diff} \tag{16}$$

The symmetric Zeta Co-CVaR measure is then defined as the average of both conditional expectations represented in (15) and (16):

$$\mathrm{Z}_{\mathrm{n,n''}}^{\mathrm{Co-CVaR(95\%)}} = \frac{1}{2} \left(\mathrm{Z}_{\mathrm{n|n''}}^{\mathrm{Co-CVaR(95\%)}} + \mathrm{Z}_{\mathrm{n''|n}}^{\mathrm{Co-CVaR(95\%)}} \right) \tag{17}$$

3.1.6. *BESS energy and power ratings*

The initial investment parameters of each BESS technology are formulated based on BESS energy and power ratings in MWh and MW. The BESS energy rating is denoted as $BESS_{MWh}^{Total}$, while the depth of discharge in MWh is represented in (18).

$$BESS_{MWh}^{DoD} = BESS_{MWh}^{Total} \times DoD\ (\%) \tag{18}$$

Furthermore, the BESS power rating for total investment in MW is calculated as:

$$BESS_{MW}^{Total} = \frac{BESS_{MWh}^{Total}}{T_{ch/di}} \tag{19}$$

Fig. 1 presents a flow diagram for determining optimal BESS investment design parameters. It starts with the collection of quarterly day-ahead LMP load nodes data for calendar year 2021–2024 and initialization of a node counter ($n = 1$). The algorithm then processes each node iteratively, applying a rolling horizon approach to obtain the average of the consecutive peak and non-peak LMPs, computing the daily delta LMP, and evaluating statistics of the return on BESS investment as Zeta. This iterative loop continues, incrementing the node counter ($n = n + 1$) until all N_{nodes} nodes are processed, resulting in a compiled set of statistical parameters, including the average, variance, and covariances of Zeta across all nodes. These aggregated statistical parameters subsequently serve as critical inputs to the BESS optimal investment design process, where both CCNS and PUO methods are developed to perform optimal BESS siting and sizing decisions, respectively. The flowchart concludes with the final step of selecting optimal BESS technology. The next section of the methodology explains the process of the CCNS method in detail, which employs an optimal cluster selection and node selection model based solely on average and variance for the BESS siting process.

3.2. CCNS method

The CCNS method is employed to identify optimal candidate nodes for BESS siting by systematically evaluating LMP characteristics. In this approach, hourly LMP data are first clustered using the k-means algorithm, grouping nodes with similar price behavior into distinct clusters. Each node within a cluster is then assessed using the INVF, which incorporates key statistical parameters, including the average (expected return) and variance (risk) for LMP-based arbitrage opportunities. By jointly considering these parameters, CCNS prioritizes nodes that exhibit high expected returns with controlled volatility. The resulting ranking enables the selection of nodes from the most favorable cluster while filtering out high-risk or unstable locations, thereby providing a robust and data-driven foundation for optimal BESS siting. The next sections will explain the step-by-step process of the CCNS method.

3.2.1. Designing the K-means clustering framework

Scaling Input Features: The input features are important for the investment decision process. Therefore, Z_n^{avg} and Z_n^{var} are used as components of the input matrix for k-means clustering and are scaled to normalized values using an n-normalizer, as represented in (20) and (21).

$$Z_n^{avg,norm} = \frac{Z_n^{avg} - \min(Z_n^{avg})}{\max(Z_n^{avg}) - \min(Z_n^{avg})} \tag{20}$$

$$Z_n^{var,norm} = \frac{Z_n^{var} - \min(Z_n^{var})}{\max(Z_n^{var}) - \min(Z_n^{var})} \tag{21}$$

where, $Z_n^{avg,norm}$ and $Z_n^{var,norm}$ are the normalized values of Z_n^{avg} and Z_n^{var} respectively.

K-means Clustering Algorithm: The k-means clustering algorithm starts with optimal selection of 'k' clusters. For this purpose, the elbow and silhouette methods are collectively applied as described in [36] and represented by (22).

$$k = \frac{k_{elbow} - k_{silhouette}}{2} \tag{22}$$

Each node is represented as a two-dimensional feature vector input, based on (20) and (21):

$$x_n = \begin{bmatrix} Z_n^{avg,norm} \\ Z_n^{var,norm} \end{bmatrix} \tag{23}$$

K-means clustering is used for partitioning the data into 'k' clusters, with the centroid of each cluster being computed as:

$$\mu_i = \frac{1}{|C_i|} \sum_{x_j \in C_i} \begin{bmatrix} Z_j^{avg,norm} \\ Z_j^{var,norm} \end{bmatrix} \tag{24}$$

where, i represents the index of the i^{th} cluster in the k-means clustering algorithm, $|C_i|$ represents the total count of nodes in the cluster i, C_i represents the set of nodes assigned to the cluster i and μ_i represents the centroid of each cluster i.While partitioning the data into 'k' clusters, the sum of squared distances between each data point and its respective cluster centroid is minimized. Therefore, based on (23) and (24), the objective function of k-means clustering is defined as:

$$\min_{C_1, C_2, \ldots, C_k} \sum\nolimits_{i=1}^{k} \sum\nolimits_{n \in C_i} \|x_n - \mu_i\|^2 \tag{25}$$

Selecting Optimal Cluster of Nodes for BESS Placement: To find the optimal cluster of nodes for BESS placement, among a total of $K_{clusters}$, the Z_k^{avg} and Z_k^{var} for all N_k nodes in the k^{th} cluster are represented by (26) and (27):

$$Z_k^{avg} = \frac{1}{N_k} \sum_{n=1}^{N_k} Z_n^{avg,norm} \tag{26}$$

$$Z_k^{var} = \frac{1}{N_k} \sum_{n=1}^{N_k} Z_n^{var,norm} \tag{27}$$

where, Z_k^{avg} is the average of $Z_n^{avg,norm}$ values for all nodes in the k^{th} cluster, Z_k^{var} is the average of $Z_n^{var,norm}$ values for all nodes in the k^{th} cluster and N_k is the total number of nodes within the k^{th} cluster. Next, the cluster score C_k for the k^{th} cluster is calculated by using (26) and (27):

$$C_k = Z_k^{avg} - Z_k^{var} \tag{18}$$

Among all the $K_{clusters}$, the cluster with the maximum value of C_k represents the optimal cluster, as it has the highest average and the lowest variance, as expressed in (29).

$$C_{opt} = max(C_k) \tag{29}$$

Finally, the m^{th} node of the optimal cluster is represented by notation (30):

$$m \in C_{opt} \tag{30}$$

In the next phase Z_m^{avg}, Z_m^{var} and $Z_m^{CVaR(95\%)}$ variables are used for 'm' optimal nodes.

3.2.2. Defining individual node value function

The Individual Node Value Function ($INVF_m$) is defined to select the top 'm' optimal LMP nodes based on the tradeoff between expected return, variance, and tail risk, as represented in (31):

$$INVF_m = Z_m^{avg} - \frac{1}{2} \times A_{risk} \times \left(Z_m^{var} + Z_m^{CVaR(95\%)}\right) \tag{31}$$

where, Z_m^{avg} is the average Zeta value for node m (expected return), Z_m^{var} is the variance of Zeta values for node m, $Z_m^{CVaR(95\%)}$ is the Zeta CVaR for the m^{th} node (downside tail risk) and A_{risk} is the risk aversion factor (higher values penalize risk more).

Next, Fig. 2 illustrates the detailed CCNS workflow, which begins with the optimal cluster selection block. This block takes as inputs the

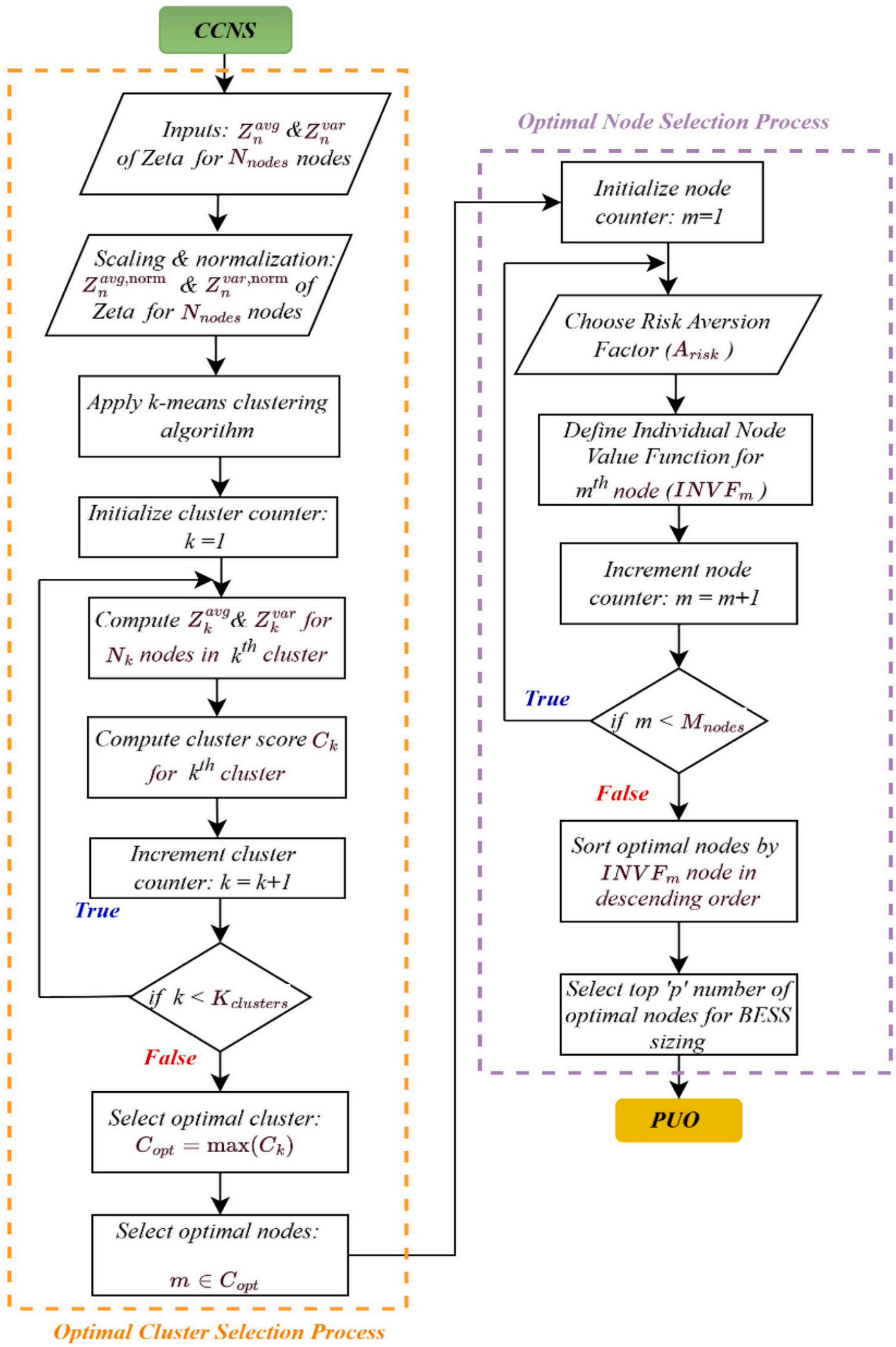

Fig. 2. CCNS method workflow.

pre-computed Zeta parameters, including the average Z_n^{avg} and variance Z_n^{var}, which are then scaled and normalized to $Z_n^{avg,norm}$ and $Z_n^{var,norm}$ for all N_{nodes} nodes. A k-means clustering algorithm is applied, initialized with a cluster counter $k = 1$, to group all network nodes. For each cluster, the average Z_k^{avg} and variance Z_k^{var} are computed, followed by the cluster score C_k. The cluster counter is incremented as $k = k + 1$, and the process repeats until all $K_{clusters}$ are processed. The optimal cluster C_{opt} is selected based on the maximum value of C_k, finalizing the set of m nodes within the optimal cluster. The second block represents the optimal node selection process using the Individual Node Value Function ($INVF_m$). The algorithm initializes a node counter $m = 1$ within C_{opt} and, incorporating a defined risk aversion factor A_{risk}, computes $INVF_m$ for each node iteratively while incrementing the counter as $m = m + 1$ until all M_{nodes} nodes are processed. The nodes are then sorted by $INVF_m$ in descending order, and the top p optimal nodes are selected for BESS sizing. The next section details the PUO, which ensures optimal siting results through a more sophisticated risk analysis that additionally incorporates the covariances of returns while considering the variables Z_p^{avg}, Z_p^{var}, Z_p^{covar}, $Z_p^{CVaR(95\%)}$ and $INVF_p$ for the top 'p' optimal nodes.

3.3. PUO method

Following node selection through CCNS, the PUO framework is applied to determine the optimal allocation of BESS capacity among the selected nodes. PUO is based on the Markowitz portfolio optimization theory, where each node is treated as an asset with associated expected

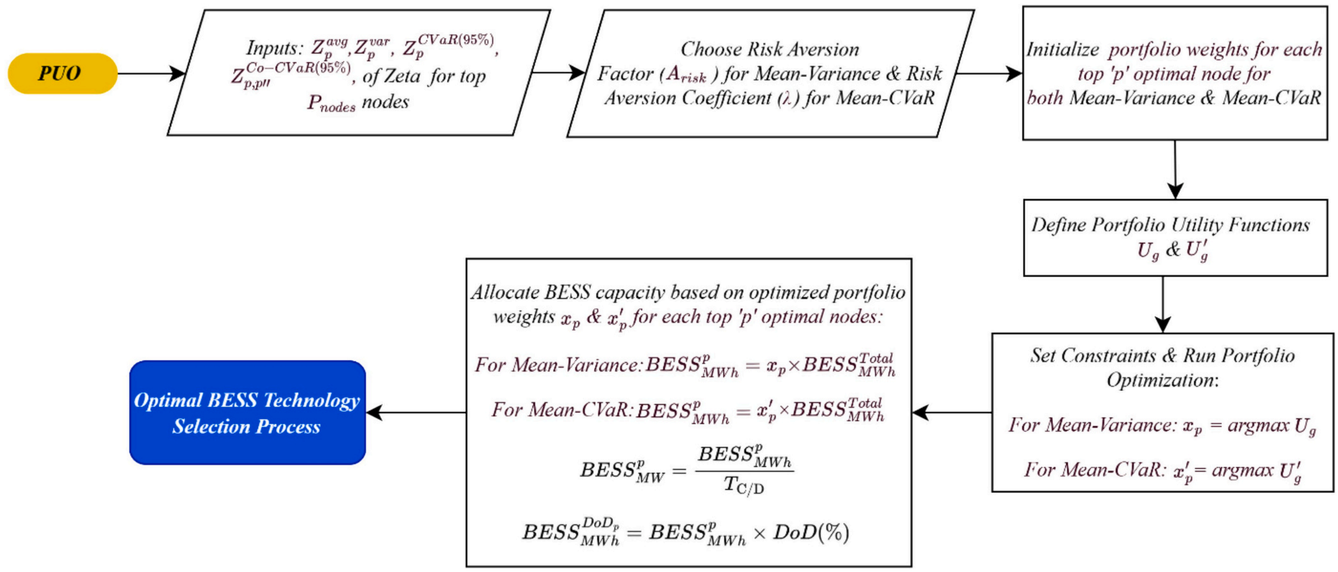

Fig. 3. PUO method workflow.

returns and risk. Unlike simple proportional allocation methods, PUO explicitly accounts for the dependence structure among node returns, allowing the model to capture temporal interdependencies in LMP behavior. In this study, two distinct portfolio optimization approaches are implemented. The first approach is the Mean-Variance Portfolio Utility Function, which uses a combination of variance and covariances as risk measures and the second approach is the Mean-CVaR Portfolio Utility Function, which replaces them with CVaR and Co-CVaR to focus exclusively on downside tail risk. Both frameworks incorporate a risk-aversion parameter, enabling flexible trade-offs between return maximization and risk mitigation. The resulting risk-adjusted portfolio weights are subsequently translated into optimal BESS capacity allocations, ensuring that sizing decisions are both economically efficient and resilient under market uncertainty. The detailed formulation and implementation of both PUO methods are presented in the following sections.

3.3.1. Defining mean-variance portfolio utility function

Based on the analysis of $INVF_p$ for top 'p' optimal nodes, Markowitz's portfolio utility function (U_g) is used to allocate optimal weights in percentage for each candidate LMP node, with no single node exceeding a 50% allocation, as represented in (32):

$$U_g = \sum_{p=1}^{P_{nodes}} x_p \times Z_p^{avg} - \frac{1}{2} \times A_{risk} \left\{ \sum_{p=1}^{P_{nodes}} Z_p^{var} + \sum_{p=1}^{P_{nodes}} \sum_{\substack{p' \neq 1 \\ p' \neq p}}^{P_{nodes}} Z_{p,p'}^{covar} \right\} \tag{32}$$

From (32), the objective function is represented as:

$$x_p = \underset{x_p}{arg\,max}\, U_g$$

Subject to constraints represented as:

$$i)\ \sum_{p=1}^{P_{nodes}} x_p = 1$$

$$ii)\ 0 \leq x_p \leq 0.5$$

where, x_p is the portfolio weights for each of the top 'p' optimal nodes and p' is the index representing a secondary or comparative node with the primary p^{th} node, used in portfolio optimization and P_{nodes} represents the total number of top selected 'p' optimal nodes.

3.3.2. Defining mean-CVaR portfolio utility function

Based on the concept explained in 3.3.1. The Mean-CVaR portfolio utility function $\left(U_g^{'}\right)$ is defined as:

$$U_g^{'} = \sum_{p=1}^{P_{nodes}} x_p^{'} \times Z_p^{avg} - \lambda \times \left(\sum_{p=1}^{P_{nodes}} \sum_{p''=1}^{P_{nodes}} x_p^{'} \times x_{p''}^{'} \times \begin{cases} Z_p^{CVaR(95\%)} & if\ p'' = p \\ Z_{p,p''}^{Co-CVaR(95\%)} & if\ p'' \neq p \end{cases} \right) \tag{33}$$

From (33), the respective objective function is represented as:

$$x_p^{'} = \underset{x_p^{'}}{arg\,max}\, U_g$$

Subject to constraints represented as:

$$i)\ \sum_{p=1}^{P_{nodes}} x_p^{'} = 1$$

$$ii)\ 0 \leq x_p^{'} \leq 0.5$$

where, $x_p^{'}$ is the Zeta CVaR portfolio weights for each of the top 'p' optimal nodes, while node p'' is the secondary or comparative node with the primary p^{th} node used in portfolio optimization, $x_p^{'}$ is the Zeta CVaR portfolio weights for each of the top 'p' optimal nodes, $x_{p''}^{'}$ represents the Zeta CVaR portfolio weights for each of the top 'p''' optimal nodes and λ is the risk aversion coefficient that quantifies the investor's willingness to trade off expected return against tail risk. A higher λ places a greater penalty on portfolio tail risk (CVaR and Co-CVaR), resulting in a more conservative allocation. Conversely, a lower λ prioritizes return maximization with less concern for extreme losses.

Table 1
Cost and performance estimates for year 2020 [37].

BESS components	Year 2020: 100 MW– 4 h system	
	LFP	**Vd**
$SB_{\$/MWh}$	165,000	261,000
$SBOS_{\$/MWh}$	38,000	52,000
$SI_{\$/MWh}$	44,000	48,000
$EPC_{\$/MWh}$	53,000	54,000
$PD_{\$/MWh}$	63,000	68,000
$PE_{\$/MW}$	63,000	115,000
$CC_{\$/MW}$	2000	2000
$GI_{\$/MW}$	20,000	20,000
$F_{O\&M}^{\$/MW-yr}$	3790	5890
$V_{O\&M}^{\$/MWh}$	512.5	512.5
$RTE_{losses}^{\$/MWh}$	5	14
DoD (%)	80	90
No. of Cycles	2000	5201
Y_b^{lc}	5.77 years (~2,107 days)	15 years (~5,479 days)
N_b^{rep}	2	–
Equivalent Full Cycle	$\frac{2,000}{2,107} = 0.95$	$\frac{5,201}{5,479} = 0.95$

3.3.3. Optimal BESS capacity sizing

For the optimal BESS capacity sizing, x_p and $x_p^{'}$ are used as the optimal portfolio weights for each top optimal node through Mean-Variance and Mean-CVaR portfolio functions, respectively. The updated BESS investment for the p^{th} node is calculated as:

$$ForMean - Variance\ PUO : BESS_{MWh}^{p} = x_p \times BESS_{MWh}^{Total} \tag{34}$$

$$ForMean - CVaR\ PUO : BESS_{MWh}^{p} = x_p^{'} \times BESS_{MWh}^{Total} \tag{35}$$

Considering the concepts from (18) and (19), the optimal BESS power rating $BESS_{MW}^{p}$ and BESS energy ratings in terms of depth of discharge $BESS_{MWh}^{DoD_p}$ for the p^{th} node is calculated as:

$$BESS_{MW}^{p} = \frac{BESS_{MWh}^{p}}{T_{ch/di}} \tag{36}$$

$$BESS_{MWh}^{DoD_p} = BESS_{MWh}^{p} \times DoD\ (\%) \tag{37}$$

Next, Fig. 3 illustrates the PUO workflow for optimal BESS sizing. The algorithm takes as inputs the Zeta parameters, including the average Z_p^{avg}, variance Z_p^{var}, and covariance $Z_{p,p'}^{\text{covar}}$ for the Mean-Variance PUO approach, along with the Conditional Value at Risk $Z_p^{\text{CVaR(95\%)}}$ and Co-Conditional Value at Risk $Z_{p,p''}^{\text{Co-CVaR(95\%)}}$ for the Mean-CVaR PUO approach, for all top selected P_{nodes} nodes, together with a defined risk aversion factors A_{risk} and risk aversion coefficient λ. Initial equal portfolio weights x_p (for Mean-Variance PUO) and $x_p^{'}$ (for Mean-CVaR PUO) are assigned to each top node, and portfolio utility functions U_g and $U_g^{'}$ are formulated within the Markowitz portfolio optimization framework. The optimization is executed to maximize U_g (Mean-Variance PUO) or $U_g^{'}$ (Mean-CVaR PUO) subject to constraints that the sum of weights equals one and no single node exceeds a 50% allocation. Upon determining the optimal weights x_p or $x_p^{'}$, the BESS capacity is allocated proportionally across the selected nodes, yielding the energy rating $\text{BESS}_{\text{MWh}}^{p}$, power rating $\text{BESS}_{\text{MW}}^{p}$, and depth-of-discharge rating $\text{BESS}_{\text{MWh}}^{\text{DoD}_p}$ for each node. The next section details the optimal process for selecting BESS technology, utilizing a techno-economic assessment to determine the best option.

3.4. Optimal BESS technology selection using techno-economic assessment

The optimal BESS technology selection is carried out through a techno-economic assessment based on NPV and IRR. For each candidate technology, capital expenditure, replacement cost, operational cost, and efficiency parameters are incorporated to evaluate long-term financial performance under different discount rates and planning horizons. NPV is used to quantify the absolute economic benefit of each technology, while IRR provides a relative measure of investment attractiveness and capital efficiency. By jointly analyzing NPV and IRR outcomes across multiple scenarios, the framework identifies BESS technologies that offer excellent profitability, robustness, and long-term viability under market uncertainty. To validate the results, two scenarios and a sensitivity analysis are conducted over a 15-year horizon, as described in the Introduction section. The next sections will provide the detailed steps of the optimal BESS technology selection process.

3.4.1. Quantifying BESS energy rating ($/MWh) and power rating ($/MW) components

In this section, a structured techno-economic assessment is conducted to evaluate and compare multiple BESS technologies for optimal deployment. The analysis focuses on calculating the NPV and IRR of each technology over a certain yearly planning horizon, incorporating technology-specific parameters such as capital costs, life cycles, and storage block replacement schedules. This approach dynamically accounts for discounted cash flows and time-based replacement costs, ensuring a more realistic estimation of long-term net benefits. Quantifying the financial metrics, including $/MWh and $/MW components of BESS technologies, helps to identify the most economically feasible BESS technology that aligns with both operational requirements and investment efficiency. The details of the components are explained in the parameters, symbols, and notations of the paper.

For optimal selection of BESS technologies, two predominant BESS technologies, including Lithium-Ferro-Phosphate-Lithium-ion (LFP) and Vanadium Redox Flow (Vd) are selected to design an optimal BESS technology selection model based on NPV and IRR. The life cycle of each BESS technology is different; therefore, the suggested model involves a maximum number of years between storage block (SB) replacement of each BESS technology. The cost and performance metrics for the year 2020 for the respective BESS technologies for a 100 MW–4 h BESS are provided in Table 1. The lifespan benchmarks for BESS technologies assume a daily charge/discharge cycle, as cited in [37].

Table 1 demonstrates that Vd exhibits the longest life cycle among all BESS technologies. $Y_{max}^{lc} = 15$ years. Furthermore, Y_b^{lc} represents the duration corresponding to the life cycle of b^{th} BESS technology in the years. However, during the longest life cycle of BESS technology, the SB replacements required for the b^{th} BESS technology, N_b^{rep}, are calculated as:

$$N_b^{rep} = \frac{Y_{max}^{lc}}{Y_b^{lc}} - 1 \tag{38}$$

To account for the replacements over the Y_{max}^{lc} years, the specific years in which the storage blocks are replaced must be precisely identified. These years are represented as the scheduled replacement periods for the b^{th} BESS technology, as represented in notation (39).

$$S_{BR} = \{y_r \mid r = 1, 2, 3 \ldots, N_b^{rep}\} \tag{39}$$

where, S_{BR} is the set of storage block replacement years, r is the replacement index for the b^{th} BESS technology and $y_r = 1 + (Y_b^{lc} \times r)$ representing the year in which a storage block replacement occurs.

3.4.2. Calculating BESS total operating cost

For each BESS technology, the total annual operating cost includes the cost of Fixed O&M, Variable O&M, System RTE Losses for the p^{th} node, and the b^{th} BESS technology, as represented in (40), (41), and (42).

$$F_{O\&M}(\$) = F_{O\&M}^{\$/MW-yr} \times BESS_{MW}^{Total} \tag{40}$$

$$V_{O\&M}(\$) = V_{O\&M}^{\$/MWh} \times BESS_{MWh}^{Total} \times 365 \tag{41}$$

$$RTE_{loss}(\$) = \left\{ RTE_{losses}^{\$/MWh} \times \left(BESS_{MWh}^{Total} \times 0.1 \right) \right\} \times 365 \tag{42}$$

It is worth noting that a 10% RTE loss is assumed in (42). Using (40), (41), and (42), the total annual operation cost in \$ over the useful life of the storage block for the p^{th} node and the b^{th} BESS technology is calculated as:

$$C_{p,b}^{Opr} = F_{O\&M}(\$) + V_{O\&M}(\$) + RTE_{loss}(\$) \tag{43}$$

3.4.3. Calculating BESS total installation, replacement and salvage cost

For each BESS technology, the total installation cost includes both \$/MWh and \$/MW components for the p^{th} node and the b^{th} BESS technology, as represented in (44) and (45), respectively.

$$I_{\$/MWh} = SB_{\$/MWh} + SBOS_{\$/MWh} + SI_{\$/MWh} + EPC_{\$/MWh} + PD_{\$/MWh} \tag{44}$$

$$I_{\$/MW} = PE_{\$/MW} + CC_{\$/MW} + GI_{\$/MW} \tag{45}$$

By using (44) and (45), the total initial installation cost in \$ for the p^{th} node and the b^{th} BESS technology is calculated as:

$$C_{p,b}^{Ins} = \left(I_{\$/MWh} \times BESS_{MWh}^{p} \right) + \left(I_{\$/MW} \times BESS_{MW}^{p} \right) \tag{46}$$

A single storage block replacement cost is based on the number of replacements $\left(N_b^{rep} \right)$ will be required for each BESS technology under the specific y_r years. This replacement cost for the p^{th} node and b^{th} BESS technology is calculated as:

$$C_{p,b}^{Rep} = SB_{\$/MWh} \times BESS_{MWh}^{p} \tag{47}$$

Next, a 5% salvage value is applied to the SB cost to account for recoverable material value at the end of SB life cycle. This salvage cost for the p^{th} node and the b^{th} BESS technology is calculated as:

$$C_{p,b}^{Sal} = SB_{\$/MWh} \times 5\% \tag{48}$$

3.4.4. Defining BESS degradation factors

To capture the long-term techno-economic performance of BESS technologies, a degradation model is essential as it links the initial siting and sizing outcomes to the progressively declining usable capacity and revenue-generating potential. Degradation in battery systems arises from two distinct mechanisms, namely calendar aging, which occurs irrespective of cycling due to time-dependent chemical instability, and cycle aging, which accumulates with each daily charge-discharge event. For LFP, the degradation behavior is characterized by using the 'LFP |Gr' model reported in [38], which separately quantifies calendar loss and cyclic loss. Based on the operational assumption of one full cycle per day mentioned by [38] and the parameters derived from Table 1, the daily calendar loss for LFP is estimated at 0.015%, while the cyclic loss reaches 1.28% per year, collectively defining the annual capacity degradation trajectory. For Vd, calendar aging is considered negligible due to the inherent stability of the vanadium electrolyte, whereas cycle-induced capacity fade is the dominant in degradation mechanism. Following the findings in [39], Vd exhibits a cyclic capacity fade of 0.44% per equivalent full cycle. These technology-specific degradation parameters are subsequently integrated into the annual net cash flow formulation, where the usable energy rating is progressively reduced based on the calendar and cyclic losses to ensure that revenue projections and replacement schedules must reflect realistic operational performance over the planning horizon.

3.4.5. Calculating annual net cash flow with degradation modeling

The annual net cash flow represents the yearly profitability of a storage investment at a given node, capturing the difference between expected annual net arbitrage revenue and operational costs. This provides a foundational input for long-term value assessments. The annual net arbitrage revenue in dollars for the p^{th} node and the b^{th} BESS technology is calculated based on the degradation characteristics of each SB over its operational life. These degradation characteristics utilize capacity losses account for both calendar aging and cyclic aging, which are technology-specific factors as defined in Section 3.4.4.

For a given SB, the first year of operation incurs no calendar loss, as the calendar aging accumulation begins from the start of operation up to the annual complete cycle. For subsequent years until the scheduled replacement year Y_b^{lc}, calendar loss accumulates progressively. Cyclic loss accumulates continuously from the first day and year onward. By integrating BESS energy ratings in terms of depth of discharge, based on the concept from (18), the annual net arbitrage revenue for the p^{th} node and the b^{th} BESS technology is given by:

$$R_{p,b}^{y} = \sum_{d=1}^{365} \left(DDL_p \times BESS_{MWh}^{DoD_p} \right) \times \left\{ 1 - \left(d \times Q_{cyc,b}^{daily} \right) \right\} \times \gamma_y \tag{49}$$

where, DDL_p represents the daily delta LMP for the p^{th} node, utilized for calculating the expected annual revenue. $R_{p,b}^{y}$ represents the annual net arbitrage revenue for the p^{th} node and the b^{th} BESS technology in year 'y' of the current storage block, where $y = 1$ corresponds to the first year of the storage block with no calendar loss, and $y \geq 2$ corresponds to subsequent Y_b^{lc} years where calendar loss accumulates progressively. $Q_{cyc,b}^{daily}$ represents the daily cyclic loss rate in % for the b^{th} BESS technology during the first year of SB, and γ_y is a calendar loss factor defined as:

$$\gamma_y = \begin{cases} 1, \ y = 1 \\ 1 - \left\{ (y-1) \times Q_{cal,b}^{annual} \right\}, 2 \leq y \leq Y_b^{lc} \end{cases} \tag{50}$$

where, $Q_{cal,b}^{annual}$ represents the calendar loss in % for the b^{th} BESS technology accumulated from the second year up to the year Y_b^{lc}. Finally, the annual net cash flow for the p^{th} node and the b^{th} BESS technology is then calculated as:

$$CF_{p,b}^{y} = R_{p,b}^{y} - C_{p,b}^{Opr} \tag{51}$$

where, $CF_{p,b}^{y}$ is the annual net cash flow for the p^{th} node and the b^{th} BESS technology for 'y' number of years.

3.4.6. Calculating NPV

In financial modeling, the NPV serves as a critical metric to evaluate the economic viability of BESS investments by quantifying the projected future cash flows in present value, enabling informed comparison across technologies and nodes. The NPV for the p^{th} node and the b^{th} BESS technology is calculated in \$. The $NPV_{P_{nodes},b}$ for the b^{th} BESS technology across all nodes $(p \in P_{nodes})$ is the sum of the NPV of all P_{nodes}, as represented in (52) and (53):

$$NPV_{p,b} = -C_{p,b}^{Ins} + \sum_{y=1}^{Y_{max}^{lc}} \frac{CF_{p,b}^{y}}{(1+DR)^{Y_{max}^{lc}}} - \sum_{y_r \in S_{BR}} \frac{C_{p,b}^{Rep}}{(1+DR)^{y_r}} + \sum_{y_r \in S_{BR}} \frac{C_{p,b}^{Sal}}{(1+DR)^{y_r}} \tag{52}$$

$$NPV_{P_{nodes},b} = \sum_{p=1}^{P_{nodes}} NPV_{p,b} \tag{53}$$

where, DR represents the discount rate, $NPV_{p,b}$ is the NPV for the p^{th} node and the b^{th} BESS technology, $NPV_{P_{nodes},b}$ is the total NPV for all P_{nodes} nodes and b^{th} BESS technology and the set S_{BR} ensures that storage block

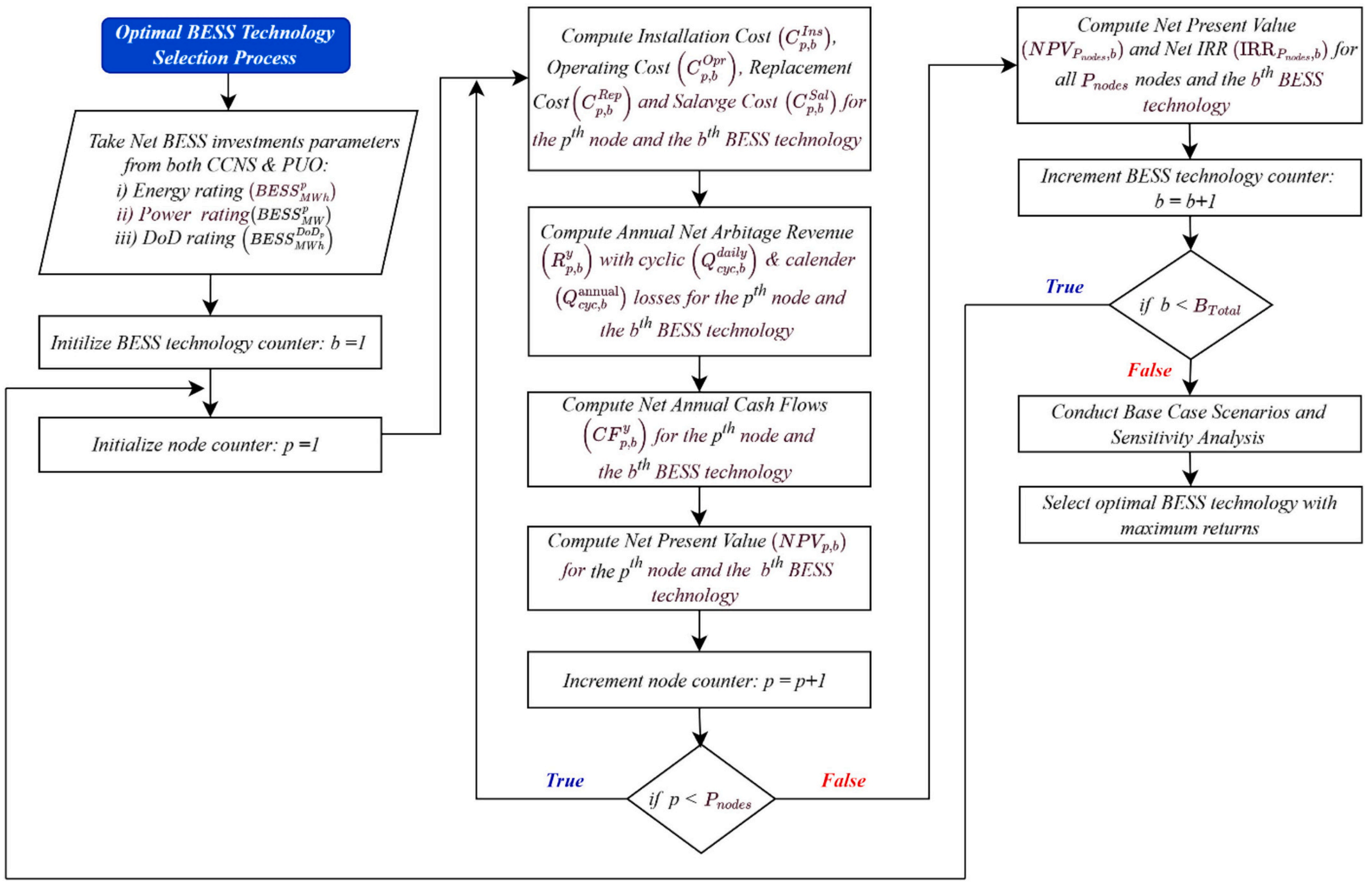

Fig. 4. Workflow of Optimal BESS Technology Selection Process.

replacements are appropriately timed and discounted in the NPV formulation for each node and BESS technology.

3.4.7. Calculating net IRR

The IRR is used to evaluate the financial performance of BESS technology by identifying the discount rate at which the NPV of all future cash flows equals zero, which indicates the expected profitability and attractiveness among multiple BESS technologies. For calculating net IRR, annual net cash flows, total installation cost for all P_{nodes} nodes, and the b^{th} BESS technology is calculated in $ as represented in (54–57):

$$CF^{y}_{P_{nodes},b} = \sum_{p=1}^{P_{nodes}} CF_{p,b} \tag{54}$$

$$C^{Ins}_{P_{nodes},b} = \sum_{p=1}^{P_{nodes}} C^{Ins}_{p,b} \tag{55}$$

$$C^{Rep}_{P_{nodes},b} = \sum_{p=1}^{P_{nodes}} C^{Rep}_{p,b} \tag{56}$$

$$C^{Sal}_{P_{nodes},b} = \sum_{p=1}^{P_{nodes}} C^{Sal}_{p,b} \tag{57}$$

As discussed, NPV is zero for IRR, therefore, (53) becomes:

$$NPV_{P_{nodes},b} = 0 \tag{58}$$

Finally, considering the (54–58), net IRR for all P_{nodes} nodes and the b^{th} BESS technology is calculated in %, as represented in (59):

$$0 = -C^{Ins}_{P_{nodes},b} + \sum_{y=1}^{Y^{lc}_{max}} \frac{CF^{y}_{P_{nodes},b}}{\left(1 + IRR_{P_{nodes},b}\right)^{Y^{lc}_{max}}} - \sum_{y_r \in S_{BR}} \frac{C^{Rep}_{P_{nodes},b}}{\left(1 + IRR_{P_{nodes},b}\right)^{y_r}} + \sum_{y_r \in S_{BR}} \frac{C^{Sal}_{P_{nodes},b}}{\left(1 + IRR_{P_{nodes},b}\right)^{y_r}} \tag{59}$$

where, $CF^{y}_{P_{nodes},b}$ is the annual net cash flow, $C^{Ins}_{P_{nodes},b}$ is the total installation cost, $C^{Rep}_{P_{nodes},b}$ is the total replacement cost and $IRR_{P_{nodes},b}$ is the net internal rate of return for all P_{nodes} nodes and the b^{th} BESS technology.

Fig. 4 presents the optimal BESS technology selection process, which follows the siting and sizing determinations from both CCNS and PUO methodologies. The process begins by taking the total BESS investment parameters, including energy rating $BESS^{p}_{MWh}$, power rating $BESS^{p}_{MW}$, and depth-of-discharge rating DoD, from previous stages. The BESS technology counter is initialized as $b = 1$, and the node counter is initialized as $p = 1$ for the first BESS technology and top optimal node respectively. For each combination of node 'p' and technology 'b', the installation cost $C^{Ins}_{p,b}$, operating cost $C^{Opr}_{p,b}$, replacement cost $C^{Rep}_{p,b}$, and salvage cost $C^{Sal}_{p,b}$ are computed, followed by the annual net arbitrage revenue $R^{y}_{p,b}$ incorporating cyclic loss $Q^{daily}_{cyc,b}$ and calendar loss $Q^{annual}_{cal,b}$. The net annual cash flow $CF^{y}_{p,b}$ and net present value $NPV_{p,b}$ are then calculated. The node counter is incremented as $p = p + 1$, and the loop continues until all total P_{nodes} nodes are processed. Upon completing all nodes for b^{th} technology, the total net present value $NPV_{P_{nodes},b}$ and net internal rate of return $IRR_{P_{nodes},b}$ are computed across all P_{nodes} nodes. The technology counter is then incremented as $b = b + 1$, and the process repeats for the next BESS technology until $b > B_{Total}$. Before final selection, two base case scenarios and their corresponding sensitivity

Table 2
ITC base rates for BESS projects under the IRA (2022–2037) [40,42].

Period	Clause	ITC rate
2022–2024	Clause 48 (as amended by IRA)	30% with full credit period.
2025–2032	Clause 48E (new credit)	30% with full credit period.
2033	Clause 48E(e)(2)(A)	Still 30% with first year of phase-out (100% of 30%).
2034	Clause 48E(e)(2)(B)	22.5% (75% of 30%) with second year of phase-out.
2035	Clause 48E(e)(2)(C)	15% (50% of 30%) with third year of phase-out.
2036–2037	Clause 48E(e)(2)(D)	0% with no credit. Any calendar year after 2035.

Table 3
Optimal cluster selection results under CCNS.

Cluster	Z_k^{avg}(max is preferred)	Z_k^{var} (min is preferred)	C_k	No. of nodes
1	0.4654	0.8845	−0.4190	38
2	0.0100	0.9997	−0.9897	158
3	0.3530	0.9354	−0.5824	140
4	0.1578	0.9863	−0.8284	49

Table 4
Optimal and non-optimal node selection under CCNS.

Optimal/non-optimal cluster	NODE	Z_p^{avg}	Z_p^{var}	$Z_p^{CVaR(95\%)}$	$INVF_p$
Optimal (1st Cluster)	EAI.EAILD.RLA	1.1231	1.8242	0.03714	−0.73822
	EAI.EAILD	1.1231	1.8242	0.03714	−0.73823
	SME.SME_LOAD	1.1212	1.8854	0.03826	−0.80248
	LAGN.LAGN	1.1977	1.9891	0.03871	−0.83006
	EES.ELILD.RLA	1.2137	2.0773	0.04065	−0.90428
	EES.ELILD	1.2137	2.0773	0.04065	−0.90428
	EES.NOPLD	1.2130	2.1176	0.04127	−0.94582
Non-optimal (2nd Cluster)	CONS.SCIT	1.1916	16.1606	0.06735	−15.03635
	WEC.WPPI	1.5443	20.2307	0.10230	−18.78865
	MIUP.WEPM	1.6540	21.6059	0.09204	−20.04395
	SIGE.CANN_MUNI	1.4125	22.4370	0.06844	−21.093
	AMIL.NORRIS	1.3811	23.3523	0.07560	−22.04684
	WPS.UMERC	1.5597	27.4632	0.10595	−26.0095
	WPS.MENOMPK	1.5240	27.7094	0.10425	−26.28963

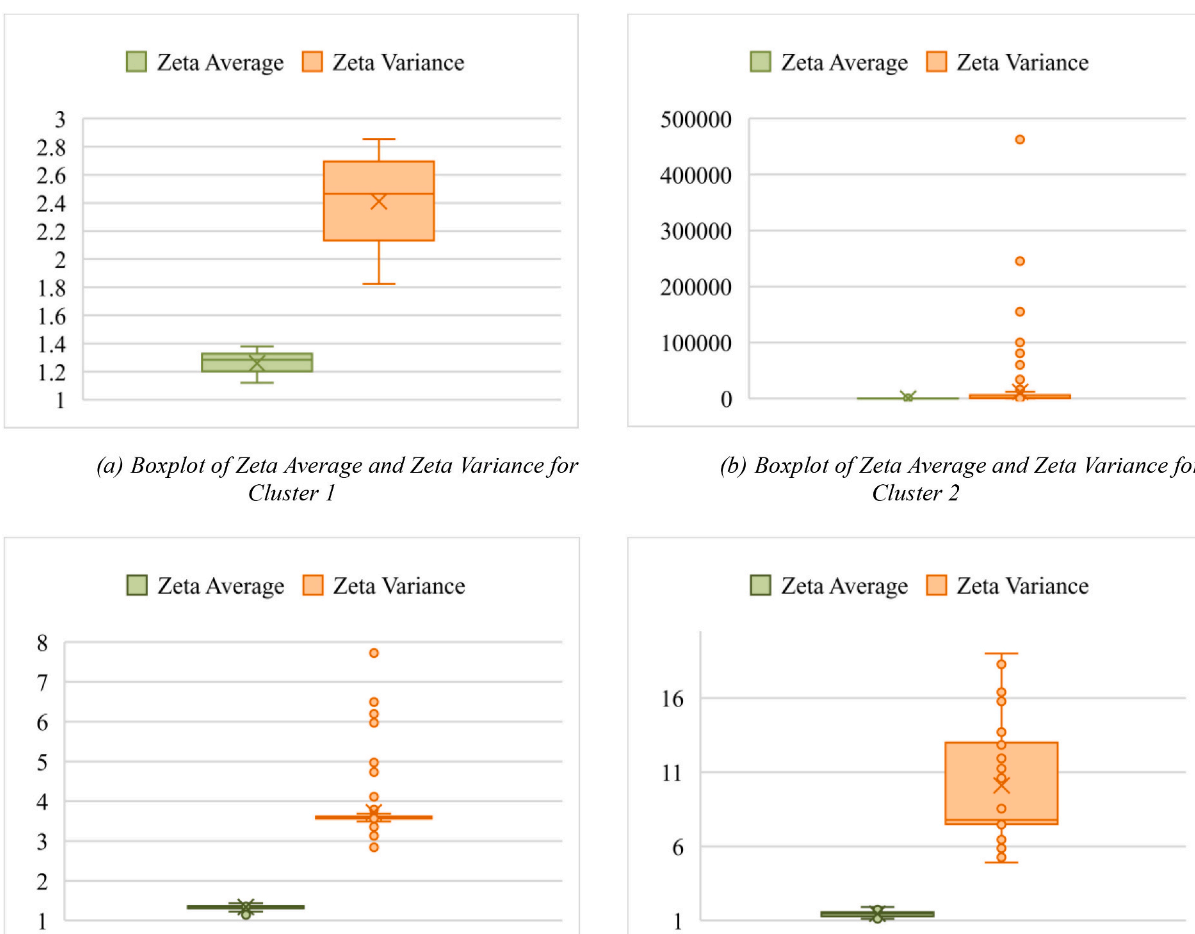

(a) Boxplot of Zeta Average and Zeta Variance for Cluster 1

(b) Boxplot of Zeta Average and Zeta Variance for Cluster 2

(c) Boxplot of Zeta Average and Zeta Variance for Cluster 3

(d) Boxplot of Zeta Average and Zeta Variance for Cluster 4

Fig. 5. (a): Boxplot of zeta average and zeta variance for cluster 1. (b): Boxplot of zeta average and zeta variance for cluster 2. (c): Boxplot of zeta average and zeta variance for cluster 3. (d): Boxplot of zeta average and zeta variance for cluster 4.

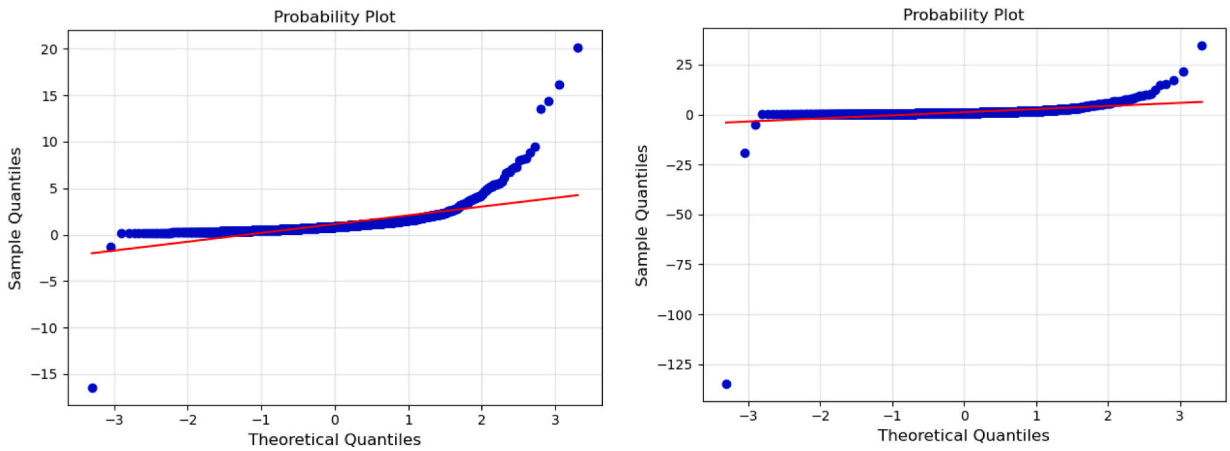

(a) Q-Q Plot of EAI.EAILD.RLA *(b) Q-Q Plot of CONS.SCIT*

Fig. 6. (a): Q-Q plot of EAI.EAILD.RLA. (b): Q-Q plot of CONS.SCIT.

Table 5
Summary of normality test (EAI.EAILD.RLA Vs CONS.SCIT).

Matrix	EAI.EAILD.RLA	CONS.SCIT
Mean	1.1231	1.1916
Standard deviation	1.3506	4.02
Skewness	+3.9370 (positive)	−26.0369 (negative)
Kurtosis	72.27	907.19
Tail behavior	Moderate heavy tails	Extreme heavy tails with left skew
Q-Q plot range	−15 to 20	−125 to 25
Shapiro-Wilk test statistics	0.4948	0.1547
P-value	0.0000	0.0000

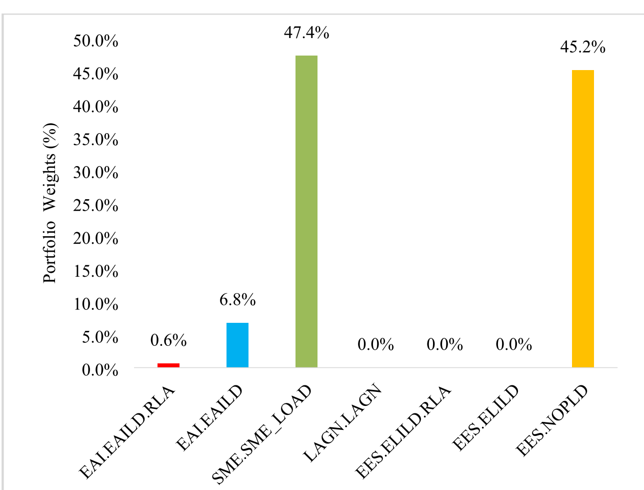

Fig. 7. Portfolio weights (%) of the top seven selected nodes (Mean-Variance PUO).

analyses are conducted to evaluate the robustness of each technology under varying market, regulatory and operational conditions. Finally, all B_{Total} technologies are compared based on $NPV_{P_{nodes},b}$ and $IRR_{P_{nodes},b}$, and the optimal BESS technology with maximum returns is selected based on the defined scenarios and sensitivity analysis.

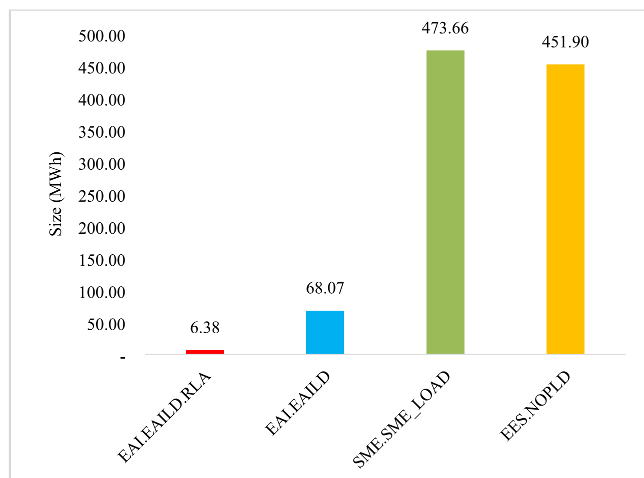

Fig. 8. Maximum optimal allocations in MWh across the top four nodes (Mean-Variance PUO).

3.5. Defining base scenarios and sensitivities

To evaluate the economic viability of BESS investments under different market and policy conditions, two base scenarios are developed alongside sensitivity analyses, as discussed in next sections.

3.5.1. Without investment tax credit (ITC) scenario

This scenario covers the capital cost trajectory of a grid-connected BESS project without considering Investment Tax Credit (ITC) framework, established under the Inflation Reduction Act (IRA) 2022, as detailed in [40]. According to a study by [41], the battery storage projects cost in $/kWh experienced an average annual cost reduction of 20% per year from 2014 to 2024, driven by annual installations exceeding 80% growth per year. Therefore, assuming the same trend, the planning horizon spans from 2020 to 2037 are developed by applying a 20% reduction to the BESS installation cost only in $/MWh per year to reflect observed market trends. This cost reduction trajectory is incorporated into the baseline to represent realistic market dynamics in the absence of policy-driven incentives. All other cost components, including installation cost in $/MW and operating costs are considered same throughout the projections in the base investment model of Without ITC scenario.

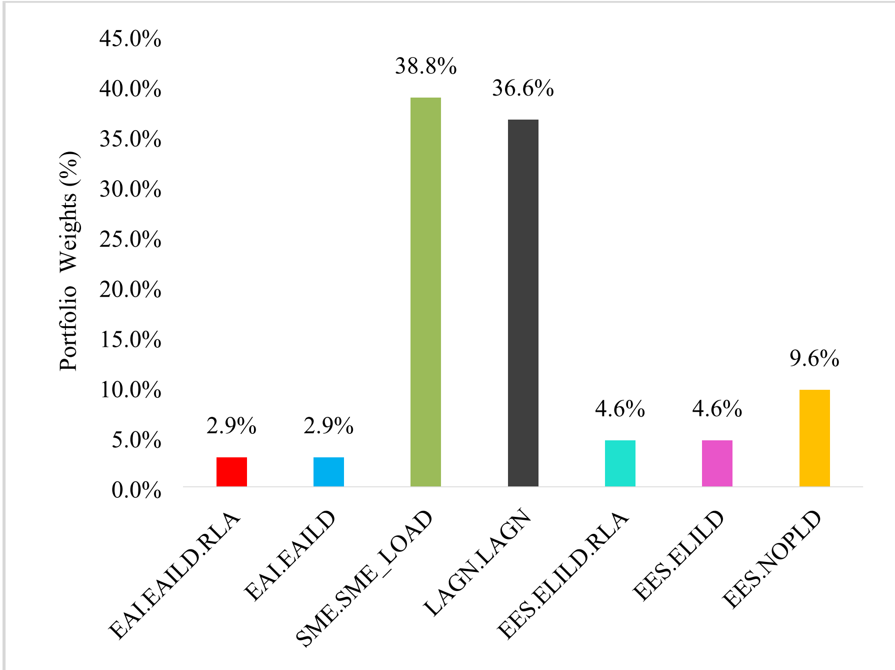

Fig. 9. Portfolio weights (%) of the top seven selected nodes (Mean-CVaR PUO).

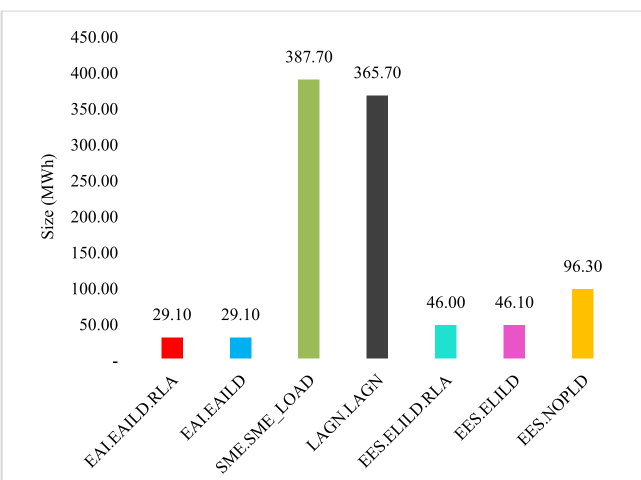

Fig. 10. Maximum optimal allocations in MWh across the top seven selected nodes (Mean-CVaR PUO).

3.5.2. With investment tax credit (ITC) scenario

In this scenario, the ITC framework is established to capture the capital cost projections of a grid-connected BESS project. The analysis covers two different tax credit regimes set up by the IRA as discussed in section 3.5.1. Under ITC, from January 1, 2022, to December 31, 2024, energy storage projects can get a tax credit under Section 48 of the Internal Revenue Code, as amended by the IRA. This credit is 30% of the project cost, but only if the project follows certain labor rules like paying fair wages and training workers. Starting on January 1, 2025, the IRA introduces a new technology-neutral credit called the “Clean Electricity Investment Credit” under Section 48E. This credit also gives 30% of the project cost, but again only if the labor rules are followed. The credit starts to phase-out after 2032, or when U.S. greenhouse gas emissions from electricity drop to 25% of the level in 2022, whichever comes later [42]. Under Section 48E(e)(2)(A), the full 30% credit is available for projects that begin construction before January 1, 2033. The phase-out begins in 2033, with the full 30% credit still applying in that year, followed by reduced rates in subsequent years, as described in Table 2.

The With ITC scenario, a 30% Investment Tax Credit (ITC) is applied annually from 2022 to 2033 to both the \$/MW and \$/MWh components of the BESS installation cost in the Without ITC scenario. The only exception is the grid integration cost (\$/MW), which remains unchanged, as ITC does not apply to costs incurred outside the BESS project. However, in 2034 and 2035, the credit amount decreases gradually according to the phase-out percentages. From 2036 to 2037, the projections align with those in Without ITC scenario.

3.5.3. Setting sensitivity analysis parameters

To assess the financial resilience of BESS technologies under varying market conditions, a key area that needs to be addressed is the energy arbitrage fluctuations, which can be easily accessed through DDL. Therefore, a sensitivity analysis is conducted around both base scenarios using the DDL as the key parameter. The portfolio optimization process allocates greater weights to nodes with higher return potential, while the risk aversion factor ensures diversification to mitigate volatility. This allows a suitable potential for energy arbitrage at the same time where storage systems buy electricity during cheap hours and sell it when expensive. However, increasing investments aggressively in BESS can lower the high price differences over time, which might reduce the profits that make these projects worth investing. To analyze this effect and test how strong the investment results can change, the DDL values from 2022 to 2037 are adjusted by sensitivities of 15% increment and 15% decrement.

4. Results and discussions

The simulation results for the optimal siting and sizing of BESS are obtained using the proposed methodology. This research assumes that the investor, private owner, or system operator has just enough capital to install 1000 MWh. Therefore, our proposed methodologies discover the BESS allocation of 1000 MWh among the optimal sites (nodes). Nevertheless, our proposed mathematical modeling is generic and can work for any BESS investment capacity. The node names have been taken from available data and correspond to actual nodes in particular

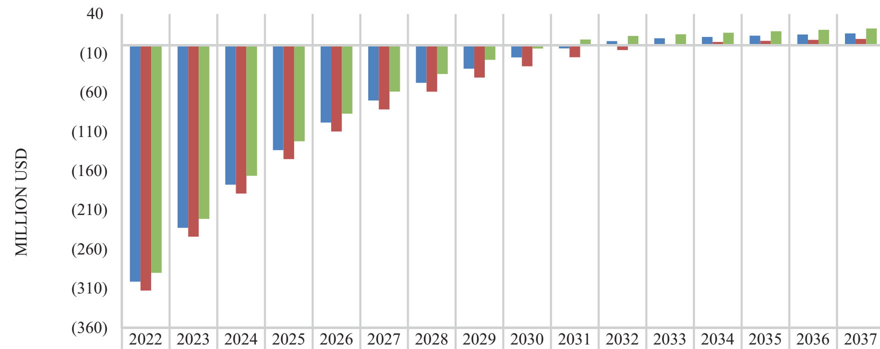

	2022	2023	2024	2025	2026	2027	2028	2029	2030	2031	2032	2033	2034	2035	2036	2037
NPV (Without ITC)	(301)	(233)	(178)	(134)	(99)	(70)	(48)	(30)	(15)	(4)	5.4	9.0	10.7	12.3	13.8	15.2
NPV (15% DDL Reduction)	(313)	(244)	(189)	(145)	(110)	(82)	(59)	(41)	(27)	(15)	(6)	1.4	4.4	5.7	7.0	8.2
NPV (15% DDL Increment)	(290)	(221)	(166)	(122)	(87)	(59)	(37)	(18)	(4)	7.5	12.1	14.1	16.1	18.0	19.8	21.5

Fig. 11. Mean-Variance PUO NPV results of LFP (without ITC scenario & DDL sensitivity analysis).

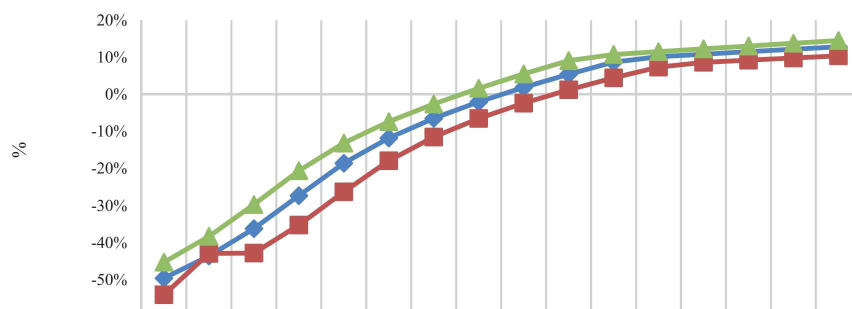

	2022	2023	2024	2025	2026	2027	2028	2029	2030	2031	2032	2033	2034	2035	2036	2037
IRR (Without ITC)	-50%	-44%	-36%	-27%	-19%	-11.8%	-6%	-2%	1.9%	5.4%	8.7%	10.1%	10.8%	11.5%	12.2%	12.8%
IRR (15% DDL Reduction)	-54%	-43%	-43%	-35%	-26%	-18%	-12%	-7%	-2%	1.2%	4.4%	7.3%	8.6%	9.2%	9.8%	10.4%
IRR (15% DDL Increment)	-45%	-38%	-30%	-21%	-13%	-7%	-3%	1.6%	5.5%	9.1%	10.7%	11.5%	12.3%	13.0%	13.8%	14.5%

Fig. 12. Mean-Variance PUO IRR results of LFP (without ITC scenario & DDL sensitivity analysis).

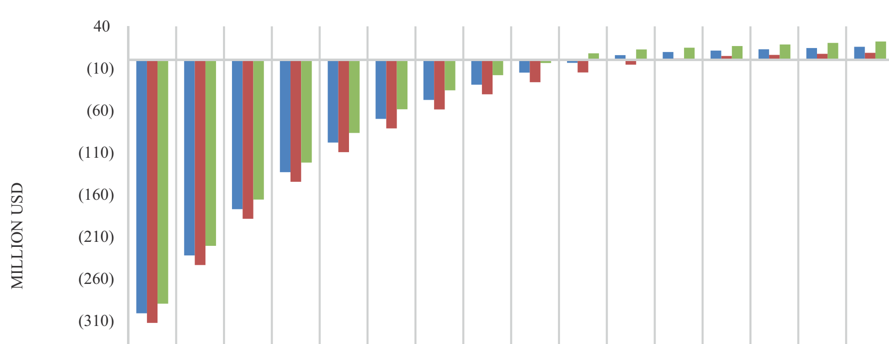

	2022	2023	2024	2025	2026	2027	2028	2029	2030	2031	2032	2033	2034	2035	2036	2037
NPV (Without ITC)	(301)	(232)	(177)	(133)	(98)	(70)	(47)	(29)	(15)	(3)	5.8	9.5	11.1	12.7	14.2	15.6
NPV (15% DDL Reduction)	(312)	(244)	(189)	(145)	(109)	(81)	(59)	(41)	(26)	(15)	(6)	1.8	4.7	6.0	7.3	8.5
NPV (15% DDL Increment)	(290)	(221)	(166)	(122)	(87)	(59)	(36)	(18)	(4)	7.9	12.6	14.6	16.6	18.5	20.3	21.9

Fig. 13. Mean-CVaR PUO NPV results of LFP (without ITC scenario & DDL sensitivity analysis).

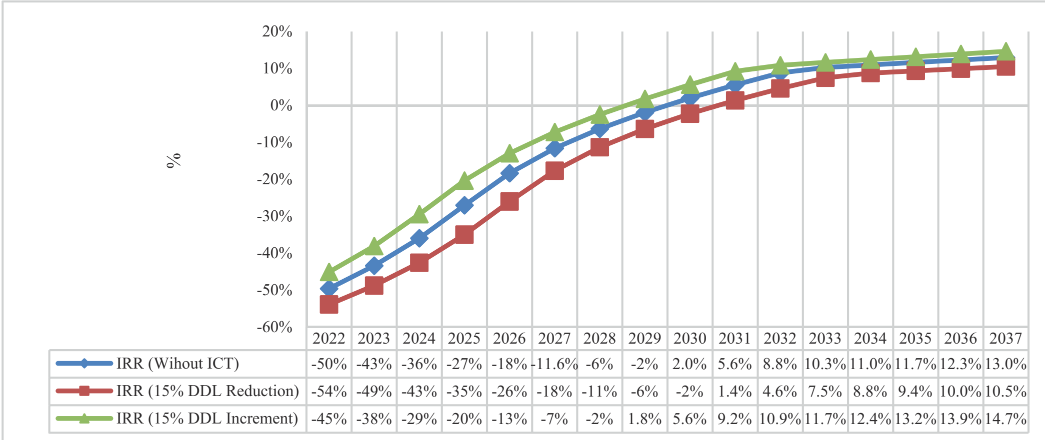

	2022	2023	2024	2025	2026	2027	2028	2029	2030	2031	2032	2033	2034	2035	2036	2037
IRR (Wihout ICT)	-50%	-43%	-36%	-27%	-18%	-11.6%	-6%	-2%	2.0%	5.6%	8.8%	10.3%	11.0%	11.7%	12.3%	13.0%
IRR (15% DDL Reduction)	-54%	-49%	-43%	-35%	-26%	-18%	-11%	-6%	-2%	1.4%	4.6%	7.5%	8.8%	9.4%	10.0%	10.5%
IRR (15% DDL Increment)	-45%	-38%	-29%	-20%	-13%	-7%	-2%	1.8%	5.6%	9.2%	10.9%	11.7%	12.4%	13.2%	13.9%	14.7%

Fig. 14. Mean-CVaR PUO IRR results of LFP (without ITC scenario & DDL sensitivity analysis).

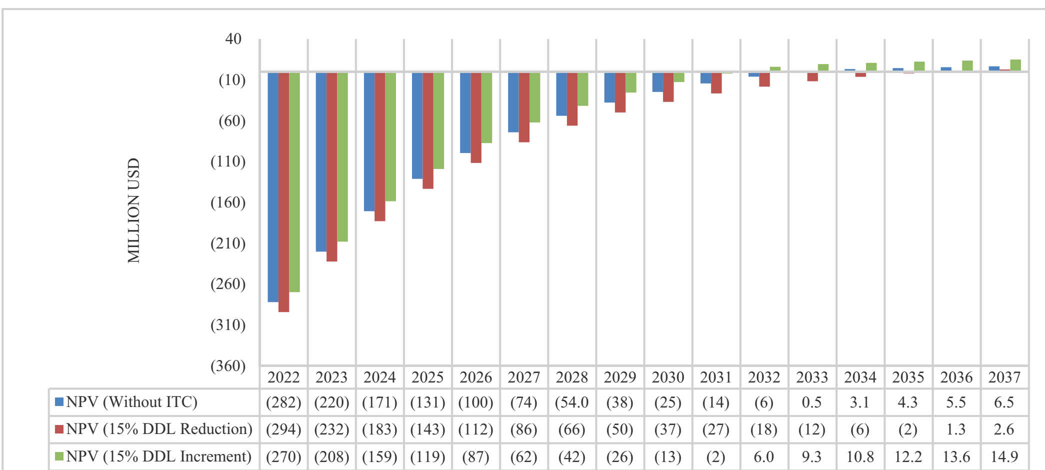

	2022	2023	2024	2025	2026	2027	2028	2029	2030	2031	2032	2033	2034	2035	2036	2037
NPV (Without ITC)	(282)	(220)	(171)	(131)	(100)	(74)	(54.0	(38)	(25)	(14)	(6)	0.5	3.1	4.3	5.5	6.5
NPV (15% DDL Reduction)	(294)	(232)	(183)	(143)	(112)	(86)	(66)	(50)	(37)	(27)	(18)	(12)	(6)	(2)	1.3	2.6
NPV (15% DDL Increment)	(270)	(208)	(159)	(119)	(87)	(62)	(42)	(26)	(13)	(2)	6.0	9.3	10.8	12.2	13.6	14.9

Fig. 15. Mean-Variance PUO NPV results of Vd (without ITC scenario & DDL sensitivity analysis).

areas of the MISO grid, but the names of the areas are not publicly known. Moreover, the framework assumes a DoD of 80%, while the $T_{ch/di}$ is fixed at 4 h. This 4-h duration is selected based on industry trends, as it has historically captured most of the electricity market for storage services, as discussed in [35]. Given that LMP data has been collected for four years, the net annual cash flow used in this study is calculated as the average of the cash flows from those four years.

Two portfolio optimization approaches are implemented to determine BESS capacity allocation, i-e; Mean-Variance PUO and Mean-CVaR PUO. For the Mean-Variance PUO, a risk aversion factor of $A_{risk} = 2$ is applied, focusing on total volatility reduction. For the Mean-CVaR PUO, the optimal risk aversion coefficient is defined as $\lambda = 35$. The Mean-CVaR PUO framework explicitly incorporates CVaR for standalone tail risk and Co-CVaR for pairwise tail dependence among nodes, capturing extreme loss behavior during volatile market conditions that traditional variance-based methods overlook.

The results offer insights into financial viability under both portfolio approaches, conducting NPV and IRR analysis based on the cost structure of a 100 MW BESS system at a 7% discount rate. The analysis is conducted under two base case scenarios including without and with ITC mechanism, along with sensitivity analyses applying 15% incremental and reduction adjustments to DDL values to assess the benefits of investment outcomes under varying market conditions over the planning horizon from 2022 to 2037.

4.1. CCNS method results

4.1.1. Optimal cluster selection results under CCNS

The CCNS was applied to determine the optimal selection of nodes and their proportional sizing for the selected optimal nodes. After performing k-means clustering, four clusters were identified using the silhouette and elbow methods, as described in (15). From these four clusters, 38 optimal nodes were selected from the optimal cluster, which is the 1st cluster. The results of the optimal cluster are presented in Table 3.

Figs. 5(a) to 5(d) present the box-plot distributions of Zeta Average and Zeta Variance for the four clusters obtained under the CCNS framework. Among all clusters, Cluster 1 (Fig. 5a) exhibits the highest Zeta Average and relatively lower Zeta Variance as compared to other clusters, indicating consistently high and stable returns across the selected nodes. In contrast, Cluster 2 (Fig. 5b) shows severe scattering in Zeta Variance with long whiskers and extreme outliers, implying high

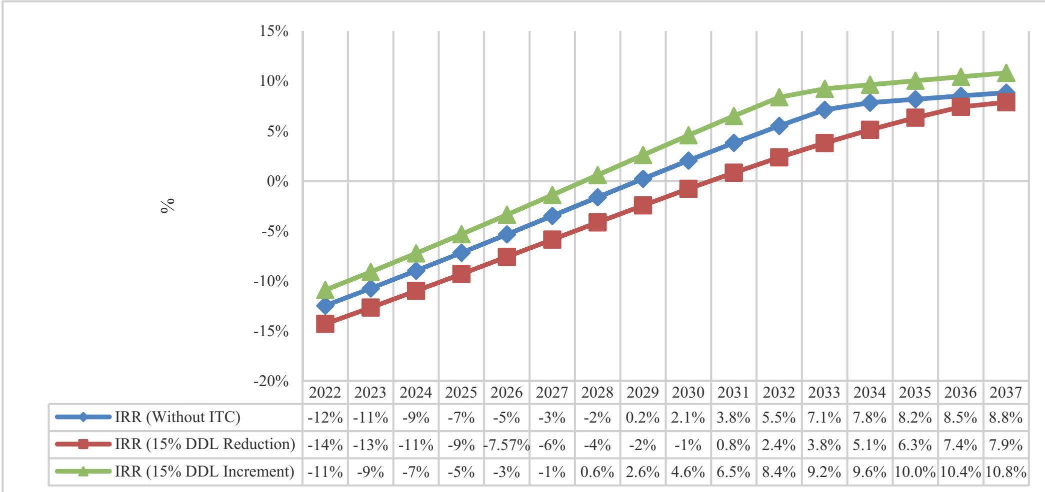

	2022	2023	2024	2025	2026	2027	2028	2029	2030	2031	2032	2033	2034	2035	2036	2037
IRR (Without ITC)	-12%	-11%	-9%	-7%	-5%	-3%	-2%	0.2%	2.1%	3.8%	5.5%	7.1%	7.8%	8.2%	8.5%	8.8%
IRR (15% DDL Reduction)	-14%	-13%	-11%	-9%	-7.57%	-6%	-4%	-2%	-1%	0.8%	2.4%	3.8%	5.1%	6.3%	7.4%	7.9%
IRR (15% DDL Increment)	-11%	-9%	-7%	-5%	-3%	-1%	0.6%	2.6%	4.6%	6.5%	8.4%	9.2%	9.6%	10.0%	10.4%	10.8%

Fig. 16. Mean-Variance PUO IRR results of Vd (without ITC scenario & DDL sensitivity analysis).

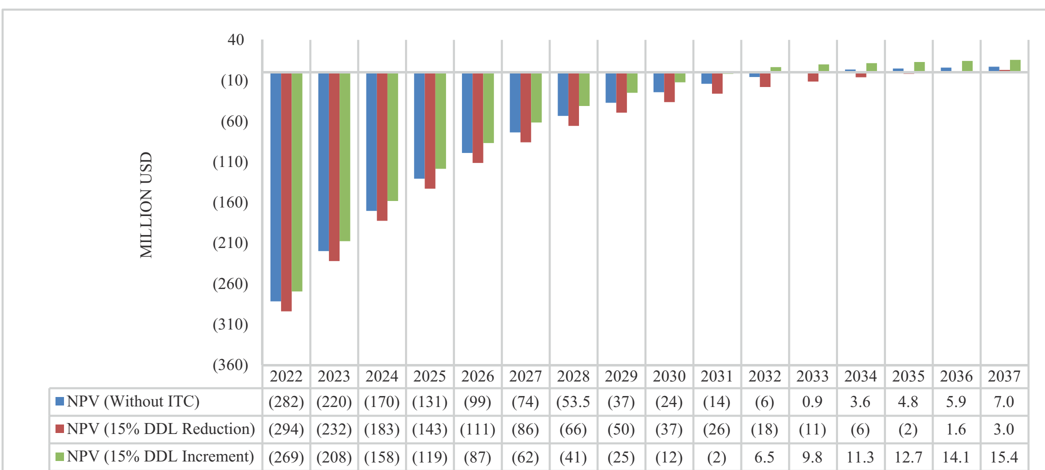

	2022	2023	2024	2025	2026	2027	2028	2029	2030	2031	2032	2033	2034	2035	2036	2037
NPV (Without ITC)	(282)	(220)	(170)	(131)	(99)	(74)	(53.5	(37)	(24)	(14)	(6)	0.9	3.6	4.8	5.9	7.0
NPV (15% DDL Reduction)	(294)	(232)	(183)	(143)	(111)	(86)	(66)	(50)	(37)	(26)	(18)	(11)	(6)	(2)	1.6	3.0
NPV (15% DDL Increment)	(269)	(208)	(158)	(119)	(87)	(62)	(41)	(25)	(12)	(2)	6.5	9.8	11.3	12.7	14.1	15.4

Fig. 17. Mean-CVaR PUO NPV results of Vd (without ITC scenario & DDL sensitivity analysis).

volatility despite acceptable mean values, and is considered the worst cluster. Cluster 3 (Fig. 5c) and Cluster 4 (Fig. 5d) indicate low Zeta Average and a larger Zeta Variance range. Collectively, based on the box-plot analysis, Cluster 1 offers the most favorable mean–variance tradeoff, thereby justifying its selection as the optimal cluster for final BESS siting, as summarized in Table 4.

Next, out of 38 nodes (selected under 1st cluster), the top seven nodes are further selected based on the INFV framework at $A_{risk} = 2$, and are discussed in the next section.

4.1.2. Optimal node selection results under CCNS

It can be observed from Table 4 that the top seven nodes selected from the optimal cluster exhibit closely clustered Z_p^{avg} values (approximately 1.12 to 1.21), indicating consistent and comparable expected performance across all selected locations. Their corresponding Z_p^{var} values remain low and tightly bound (approximately 1.82 to 2.12), reflecting minimal volatility and similar behavior. Additionally, the Z_p^{CVaR} values for these optimal nodes range from 0.0371 to 0.0413, representing a narrow and acceptable tail risk exposure of approximately 3.7% to 4.1% during extreme market conditions. In contrast, although nodes from the non-optimal cluster display Z_p^{avg} values within a similar or even higher range (1.19 to 1.65), their Z_p^{var} values increase drastically (approximately 16.16 to 27.70), indicating extreme volatility and uncertainty. Moreover, the non-optimal nodes exhibit substantially higher Z_p^{CVaR} values (0.0674 to 0.1060), reflecting tail losses more than double as compared to those of the optimal nodes, further confirming their elevated downside risk. The $INVF_p$ scores of the optimal nodes remain within a narrow and moderate range (−0.73 to −0.95), whereas the non-optimal nodes exhibit significantly more negative $INVF_p$ scores (−15.04 to −26.29), reinforcing their lower risk-adjusted performance. Therefore, the CCNS-based node selection confirms that nodes originating from the optimally identified cluster achieve a better mean–variance–tail risk balance, thereby validating the optimality of the selected nodes. The next section will explain the results of PUO based on the selected optimal nodes.

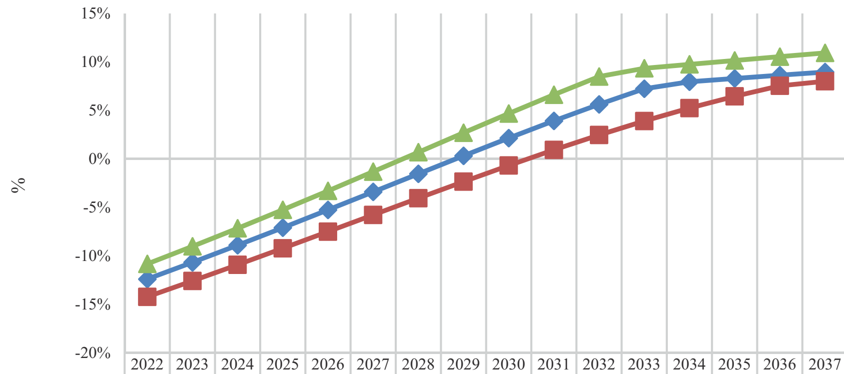

	2022	2023	2024	2025	2026	2027	2028	2029	2030	2031	2032	2033	2034	2035	2036	2037
IRR (Wihout ITC)	-12%	-11%	-9%	-7%	-5%	-3%	-2%	0.3%	2.1%	3.9%	5.6%	7.2%	8.0%	8.3%	8.6%	9.0%
IRR (15% DDL Reduction)	-14%	-13%	-11%	-9%	-7.50%	-6%	-4%	-2%	-1%	0.9%	2.5%	3.9%	5.2%	6.5%	7.5%	8.0%
IRR (15% DDL Increment)	-11%	-9%	-7%	-5%	-3%	-1%	0.7%	2.7%	4.7%	6.6%	8.5%	9.3%	9.8%	10.2%	10.5%	10.9%

Fig. 18. Mean-CVaR PUO IRR results of Vd (without ITC scenario & DDL sensitivity analysis).

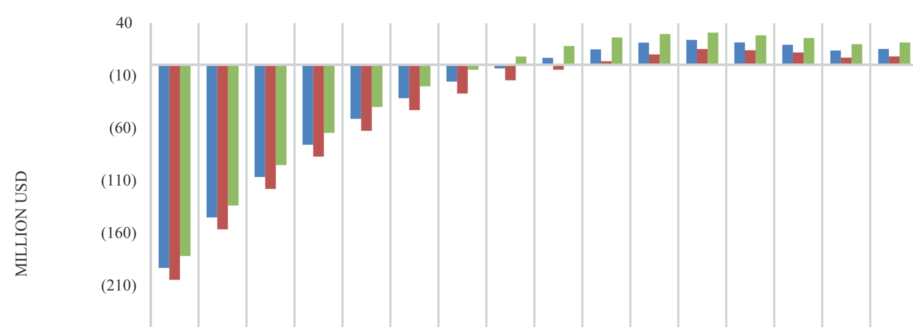

	2022	2023	2024	2025	2026	2027	2028	2029	2030	2031	2032	2033	2034	2035	2036	2037
NPV (With ITC)	(193)	(145)	(107)	(76)	(51)	(32)	(16)	(3)	7	15	21.3	23.9	21.5	19.2	13.8	15.2
NPV (15% DDL Reduction)	(205)	(157)	(118)	(87)	(63)	(43)	(27)	(15)	(5)	3.5	10.0	15.1	14.0	11.9	7.0	8.2
NPV (15% DDL Increment)	(182)	(134)	(96)	(65)	(40)	(20)	(5)	8	18	26.2	29.4	30.9	28.2	25.8	19.8	21.5

Fig. 19. Mean-Variance PUO NPV results of LFP (with ITC scenario & DDL sensitivity analysis).

4.1.3. Normality assessment of selected nodes

To validate the appropriateness of the CVaR-based risk modeling approach, a normality assessment was conducted on the return distributions of representative nodes from both optimal and non-optimal clusters. Since LMPs and consequent Zeta returns are inherently volatile and influenced by market dynamics, they are not expected to follow a normal distribution. For this analysis, one top node from the optimal cluster (EAI.EAILD.RLA) and one node from the non-optimal cluster (CONS.SCIT) were selected for comparative assessment. The results of the normality tests, including Q-Q plots and Shapiro-Wilk statistics, are presented in Figs. 6(a), 6(b) and Table 5, respectively.

Further, Table 5 presents a comparative summary of normality test results for the optimal node (EAI.EAILD.RLA) and non-optimal node (CONS.SCIT). Although both nodes reject normality (p-value = 0.0000), the Shapiro-Wilk statistic for EAI.EAILD.RLA (0.4948) is closer to 1 compared to CONS.SCIT (0.1547). A value closer to 1 indicates less deviation from normality. Therefore, EAI.EAILD.RLA exhibits relatively better behavior with moderate non-normality, while CONS.SCIT shows extreme non-normality with severe tail deviations. The EAI.EAILD.RLA exhibits a mean of 1.1231 with a standard deviation of 1.3506, skewness of +3.9370, and kurtosis of 72.27, indicating moderate heavy tails with positive skewness. In contrast, CONS.SCIT from non-optimal cluster shows a slightly higher mean of 1.1916 but with a substantially larger standard deviation of 4.02, extreme negative skewness of −26.0369, and an exceptionally high kurtosis of 907.19, reflecting extreme heavy tails with left skew. The Q-Q plot range for the optimal node spans from −15 to 20, while the non-optimal node exhibits a much wider range from −125 to 25, confirming significantly more severe tail behavior and frequent outliers in the non-optimal node. These findings confirm that while both nodes deviate from normality, the non-optimal node demonstrates substantially more extreme tail risk, justifying the use of CVaR-based models that explicitly capture downside tail behavior.

4.2. PUO method results

4.2.1. Mean-variance PUO results

The Mean-Variance PUO results are based on the portfolio-optimized weight distributions presented for the top seven selected nodes at the

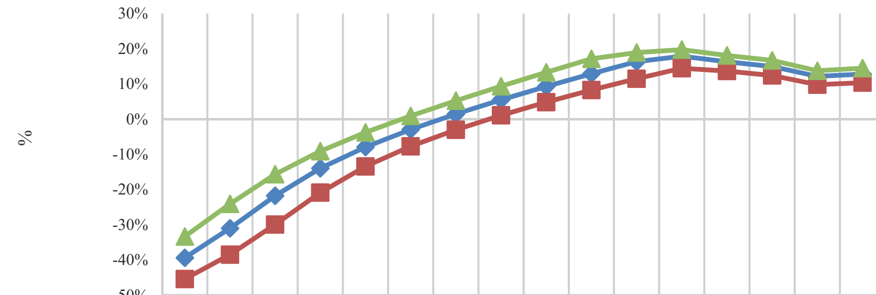

	2022	2023	2024	2025	2026	2027	2028	2029	2030	2031	2032	2033	2034	2035	2036	2037
IRR (With ITC)	-39%	-31%	-22%	-14%	-8%	-2.9%	1.5%	5.5%	9.3%	12.9%	16.3%	17.9%	16.3%	15.0%	12.2%	12.8%
IRR (15% DDL Reduction)	-45%	-38%	-30%	-21%	-13%	-8%	-3%	1.1%	4.8%	8.3%	11.5%	14.5%	13.7%	12.4%	9.8%	10.4%
IRR (15% DDL Increment)	-33%	-24%	-16%	-9%	-4%	1%	5%	9.4%	13.3%	17.2%	18.9%	19.8%	18.1%	16.7%	13.8%	14.5%

Fig. 20. Mean-Variance PUO IRR results of LFP (with ITC scenario & DDL sensitivity analysis).

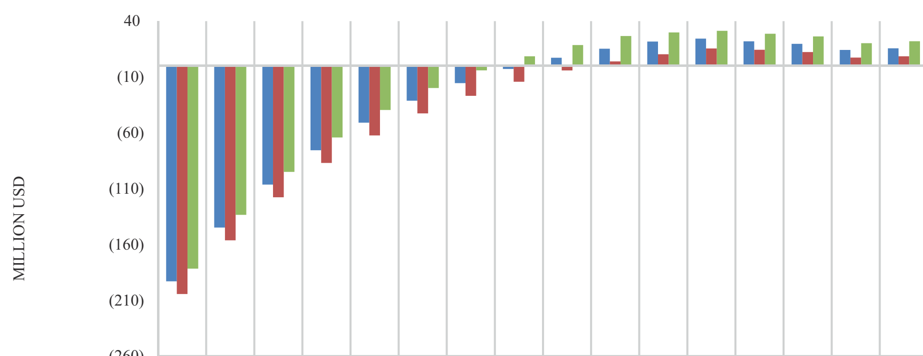

	2022	2023	2024	2025	2026	2027	2028	2029	2030	2031	2032	2033	2034	2035	2036	2037
NPV (With ITC)	(193)	(145)	(106)	(76)	(51)	(31)	(16)	(3)	7	15	21.7	24.3	21.9	19.6	14.2	15.6
NPV (15% DDL Reduction)	(204)	(156)	(118)	(87)	(62)	(43)	(27)	(14)	(4.2)	3.9	10	15.5	14.4	12.3	7.3	8.5
NPV (15% DDL Increment)	(182)	(134)	(95)	(64)	(40)	(20)	(4.1)	8.5	19	26.7	29.9	31.3	28.7	26.3	20.3	21.9

Fig. 21. Mean-CVaR PUO NPV results of LFP (with ITC scenario & DDL sensitivity analysis).

risk aversion level of $A_{risk} = 2$. Fig. 7 presents a diversified investment structure, in which the candidate nodes, such as SME.SME_LOAD and EES.NOPLD have emerged with the dominant portfolio shares of 47.4% and 45.2%, respectively, followed by EAI.EAILD with 6.8%, while the remaining nodes secure marginal weights below 1%. To ensure economic and strategic relevance, only nodes with portfolio shares exceeding 0.5% are retained for subsequent sizing analysis. These selected portfolio weights are subsequently translated into initial BESS capacity allocations, as illustrated in Fig. 8, where SME.SME_LOAD and EES.NOPLD receive the largest optimal capacities of approximately 473.66 MWh and 451.90 MWh, respectively, while EAI.EAILD is allocated 68.07 MWh and EAI.EAILD.RLA gets a smaller allocation of 6.38 MWh. This allocation preserves the relative dominance observed in the portfolio weights and demonstrates how the PUO method effectively converts risk-adjusted portfolio outcomes into physically meaningful BESS sizing decisions under risky conditions.

4.2.2. Mean-CVaR PUO results

The Mean-CVaR PUO results are based on portfolio-optimized weight distributions obtained using the CVaR and Co-CVaR risk measures at the optimal risk aversion coefficient of $\lambda = 35$. As presented in Figs. 9 and 10, the candidate nodes SME.SME_LOAD and LAGN.LAGN dominate the portfolio shares with 38.8% and 36.6%, respectively, followed by EES.NOPLD with 9.6%, while EES.ELILD, EES.ELILD.RLA, EAI.EAILD, and EAI.EAILD.RLA receive smaller allocations ranging from 2.9% to 4.6%. These portfolio weights are subsequently translated into BESS capacity allocations, where SME.SME_LOAD receives the largest allocation of approximately 387.70 MWh, followed by LAGN.LAGN with 365.70 MWh, EES.NOPLD with 96.30 MWh, EES.ELILD and EES.ELILD.RLA with 46.10 MWh and 46 MWh, respectively, and EAI.EAILD and EAI.EAILD.RLA with 29.10 MWh each. In contrast to the Mean-Variance approach, which concentrated capacity heavily on two nodes (SME.SME_LOAD and EES.NOPLD), the Mean-CVaR PUO framework produces a more diversified allocation across multiple nodes, reflecting its explicit consideration of tail risk and extreme event co-movements through the Co-CVaR PUO framework. This diversification reduces exposure to correlated tail losses and enhances portfolio resilience under volatile market conditions. The next section presents the results of the optimal BESS technology selection.

4.3. Optimal BESS technology selection results

The optimal BESS technology selection is evaluated under two scenarios. For Without ITC Scenario, as discussed in section 3.5.1, it

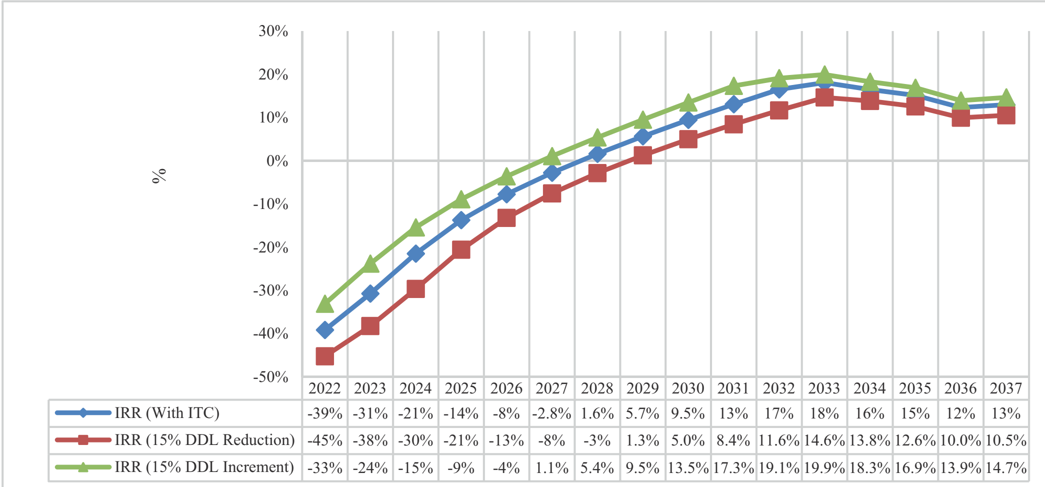

	2022	2023	2024	2025	2026	2027	2028	2029	2030	2031	2032	2033	2034	2035	2036	2037
IRR (With ITC)	-39%	-31%	-21%	-14%	-8%	-2.8%	1.6%	5.7%	9.5%	13%	17%	18%	16%	15%	12%	13%
IRR (15% DDL Reduction)	-45%	-38%	-30%	-21%	-13%	-8%	-3%	1.3%	5.0%	8.4%	11.6%	14.6%	13.8%	12.6%	10.0%	10.5%
IRR (15% DDL Increment)	-33%	-24%	-15%	-9%	-4%	1.1%	5.4%	9.5%	13.5%	17.3%	19.1%	19.9%	18.3%	16.9%	13.9%	14.7%

Fig. 22. Mean-CVaR PUO IRR results of LFP (with ITC scenario & DDL sensitivity analysis).

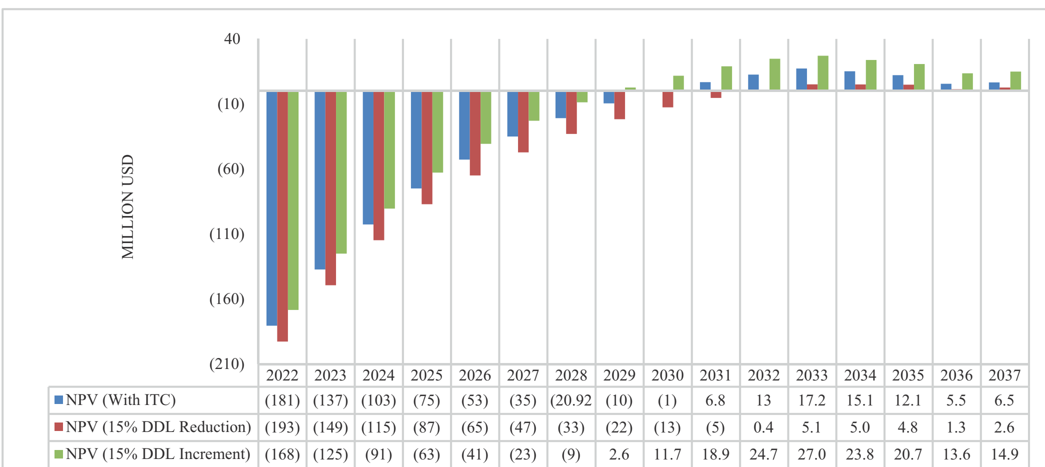

	2022	2023	2024	2025	2026	2027	2028	2029	2030	2031	2032	2033	2034	2035	2036	2037
NPV (With ITC)	(181)	(137)	(103)	(75)	(53)	(35)	(20.92	(10)	(1)	6.8	13	17.2	15.1	12.1	5.5	6.5
NPV (15% DDL Reduction)	(193)	(149)	(115)	(87)	(65)	(47)	(33)	(22)	(13)	(5)	0.4	5.1	5.0	4.8	1.3	2.6
NPV (15% DDL Increment)	(168)	(125)	(91)	(63)	(41)	(23)	(9)	2.6	11.7	18.9	24.7	27.0	23.8	20.7	13.6	14.9

Fig. 23. Mean-Variance PUO NPV results of Vd (with ITC scenario & DDL sensitivity analysis).

assumes a 20% reduction per year in installation costs from 2020 to 2037. To avoid unrealistic year-over-year jumps in financial returns, a 10% reduction cap is applied in the year following the first positive NPV and IRR, followed by a 5% cap in subsequent years, ensuring a smooth and conservative transition in profitability trends. For With ITC Scenario, a 30% year-on-year reduction is applied to Without ITC Scenario installation costs from 2022 to 2037, incorporating the phase-out percentages as discussed in Section 3.5.2. Mean-Variance and Mean-CVaR PUO methods are used for optimal BESS sizing under uncertainty. The following subsections present the comparative results for LFP and Vd technologies under both scenarios.

4.3.1. Without ITC scenario results

LFP technology results*:* Figs. 11–14 present the NPV and IRR trajectories for LFP technology from 2022 to 2037 under base and sensitivity scenarios. Considering the "Without ITC scenario", the Mean-CVaR PUO method yields consistently higher NPV values than the Mean-Variance PUO method across all years, reflecting its more conservative risk-averse perspective toward tail losses. For Mean-CVaR PUO, NPV increments from -301 Million USD (2022) to -3 Million USD (2031), while converging to 15.6 Million USD by 2037. In contrast, Mean-Variance PUO shows higher NPVs of 15.2 Million USD in 2037. Regarding IRR, Mean-CVaR PUO collectively turns positive around 2031 for all scenarios and DDL sensitivities. Mean-Variance PUO IRR follows a similar trend but remains slightly lower in early years and reaches 12.8% by 2037. However, the IRR for DDL reduction and increment sensitivities span positively from 1.2% to 14.7% under both methodologies. Overall, LFP technology remains financially viable from 2033 onward under both sizing methods, considering the Without ITC scenario and sensitivity analysis, with Mean-CVaR PUO providing a more robust risk-managed estimate.

Vd technology results*:* Figs. 15–18 illustrate the NPV and IRR outcomes for Vd technology over the same planning horizon. Under the same Without ITC scenario, the Mean-CVaR PUO method again yields higher NPV values than the Mean-Variance PUO approach across all years, as observed in LFP results. In this scenario, the Mean-CVaR PUO NPV starts at -282 Million USD (2022) and improves to -6% Million USD by 2032, and turns positive thereafter, reaching 0.9 Million USD in

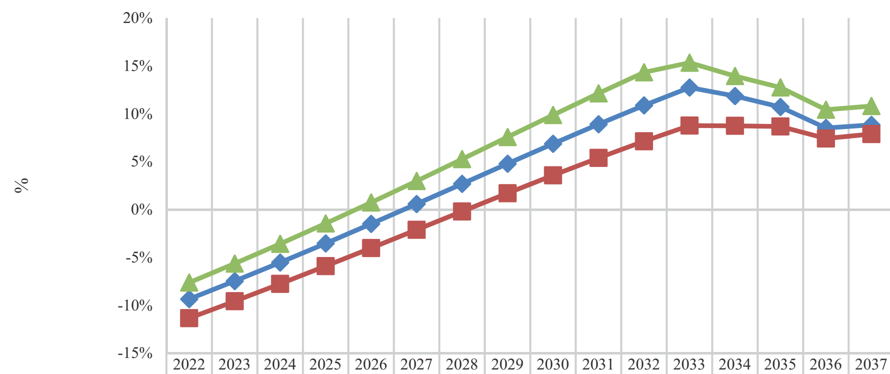

	2022	2023	2024	2025	2026	2027	2028	2029	2030	2031	2032	2033	2034	2035	2036	2037
IRR (With ITC)	-9%	-7%	-6%	-4%	-1%	0.58%	2.7%	4.8%	6.9%	8.9%	10.9%	12.7%	11.9%	10.7%	8.5%	8.8%
IRR (15% DDL Reduction)	-11%	-10%	-8%	-6%	-4.02%	-2%	0%	2%	4%	5.4%	7.1%	8.8%	8.7%	8.7%	7.4%	7.9%
IRR (15% DDL Increment)	-8%	-6%	-4%	-1%	1%	3%	5.3%	7.6%	9.9%	12.1%	14.3%	15.3%	13.9%	12.8%	10.4%	10.8%

Fig. 24. Mean-Variance PUO IRR results of Vd (with ITC scenario & DDL sensitivity analysis).

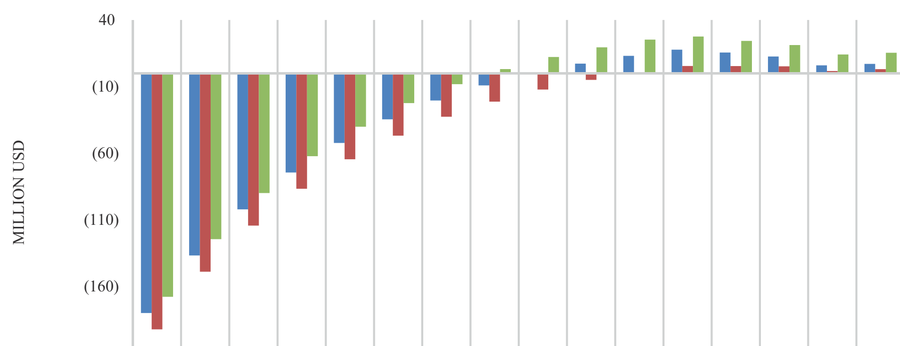

	2022	2023	2024	2025	2026	2027	2028	2029	2030	2031	2032	2033	2034	2035	2036	2037
NPV (With ITC)	(180)	(137)	(102)	(75)	(52)	(35)	(20.49	(9.1)	(0.1)	7.2	13.0	17.6	15.5	12.6	5.9	7.0
NPV (15% DDL Reduction)	(192)	(149)	(114)	(87)	(65)	(47)	(33)	(21)	(12)	(5)	0.8	5.4	5.4	5.2	1.6	3.0
NPV (15% DDL Increment)	(168)	(125)	(90)	(62)	(40)	(22)	(8)	3.1	12.2	19.4	25.2	27.5	24.3	21.2	14.1	15.4

Fig. 25. Mean-CVaR PUO NPV results of Vd (with ITC scenario & DDL sensitivity analysis).

2033. Mean-Variance PUO follows a similar but variable recovery, closing at 6.5 Million USD in 2037 under the same scenario. Analyzing the IRR performance, Mean-CVaR PUO crosses the positive threshold in 2029 (0.3%) and steadily rises to 9% by 2037. Mean-Variance PUO IRR, while slightly more restrained in early years, overtakes marginally by the end, hitting 8.8% in 2037. The DDL sensitivity analysis reveals that the 15% DDL Increment case significantly expands the upper bound of IRR from 8.8% to 10.9% in 2037, whereas the 15% DDL Reduction case widens the lower bound as low as -14% in 2022 for both Mean-Variance PUO and Mean-CVaR PUO sizing frameworks. Overall, Vd demonstrates financial viability from 2036 onward under both sizing frameworks scenarios and sensitivity analysis, with Mean-CVaR PUO offering better risk-adjusted early-stage visibility.

4.3.2. With ITC scenario results

LFP technology results*:* Figs. 19–22 present the NPV and IRR trajectories for LFP technology from 2022 to 2037 under the "With ITC scenario", including DDL sensitivity cases. A prominent observation is the pronounced gap between Mean-CVaR PUO and Mean-Variance PUO outputs, with Mean-CVaR PUO delivering substantially again higher NPVs across all years. The Mean-CVaR PUO, NPV starts at -193 Million USD (2022), turns positive by 2030 (7 Million USD), and accelerates to 15.6 Million USD in 2037. The 15% DDL Increment sensitivity amplifies this trajectory further, reaching 21.9 Million USD by 2037, while the DDL Reduction sensitivity caps at 8.5 Million USD. In Mean-Variance PUO sizing framework, NPV starts from -193 Million USD (2022) to 15.2 Million USD by 2037. On IRR performance, Mean-CVaR PUO turns positive by 2028 (1.6%) and rises sharply to 18% by 2033, with DDL Increment peaking at 14.7% and DDL Reduction reaching 10.5% in 2037. Mean-Variance PUO IRR follows a similar upward trend but remains lower across all years, reaching 12.8% by 2037, while DDL sensitivities span from -45% to 14.5%. Overall, the ITC significantly accelerates LFP's financial viability, with positive returns emerging as early as 2030–2031 under Mean-CVaR, compared to 2032–2033 under the Without ITC scenario. Mean-CVaR PUO consistently outperforms Mean-Variance PUO under the With ITC scenario and overall achieved the highest returns by 2033 under both sizing frameworks. This captures greater value from the tax credit while maintaining risk awareness.

Vd technology results*:*

Figs. 23–26 present the NPV and IRR trajectories for Vd technology from 2022 to 2037 under the same "With ITC scenario", including DDL sensitivity cases. A notable feature of Vd under the ITC is the rapid convergence of all DDL cases (Reduction, and Increment) after 2032, suggesting that the tax credit effectively neutralizes discount rate uncertainties in the medium to long term. In the Mean-CVaR PUO, NPV starts at -180 Million USD (2022) to 7.0 Million USD by 2037. The DDL Increment case follows a different trajectory, starting at -168 Million USD (2022) to 15.4 Million USD by 2037, indicating a sharper recovery

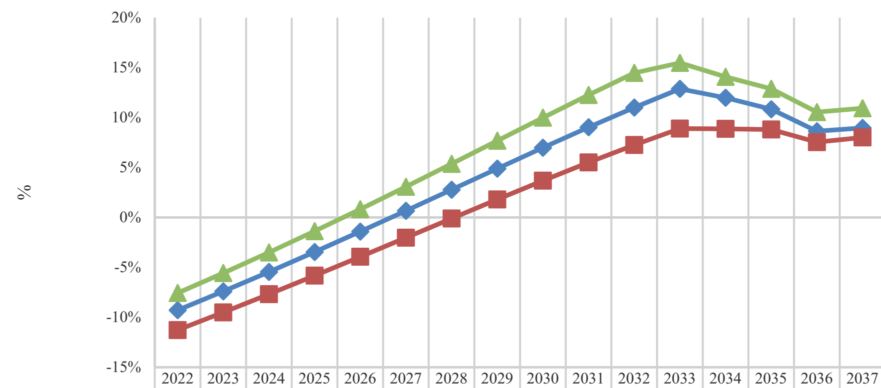

	2022	2023	2024	2025	2026	2027	2028	2029	2030	2031	2032	2033	2034	2035	2036	2037
IRR (With ITC)	-9%	-7%	-5%	-3%	-1%	0.7%	2.8%	4.9%	7.0%	9.0%	11.0%	12.9%	12.0%	10.8%	8.6%	9.0%
IRR (15% DDL Reduction)	-11%	-10%	-8%	-6%	-3.94%	-2.0%	-0.1%	1.8%	3.7%	5.5%	7.3%	8.9%	8.9%	8.8%	7.5%	8.0%
IRR (15% DDL Increment)	-8%	-6%	-4%	-1%	1%	3%	5.4%	7.7%	10.0%	12.3%	14.5%	15.5%	14.1%	12.9%	10.5%	10.9%

Fig. 26. Mean-CVaR PUO IRR results of Vd (with ITC scenario & DDL sensitivity analysis).

path. On contrary, the Mean-Variance PUO shows consistently lower NPVs starting at -181 Million USD (2022) to 6.5 Million USD by 2037. On IRR performance, Mean-CVaR PUO turns positive remarkably early by 2027 (0.7%) and rises steadily to 13% by 2033 before moderating to 9% by 2037, influenced by the phase-out of tax credits. The DDL Increment sensitivity under Mean-CVaR PUO achieves the highest peak IRR of 15.5% in 2033. Mean-Variance PUO IRR follows a similar but consistently reaching 15.3% by 2033. Overall, Vd under the With ITC scenario maintains positive NPV across all years, a completely contrast to its Without ITC performance, with Mean-CVaR PUO capturing higher early-stage value as compared to while Mean-Variance PUO BESS siting framework.

5. Conclusions, limitations, and way forward

From the overall comparative analysis, it becomes clear that the CCNS method has successfully determined the optimal and non-optimal candidate nodes by jointly evaluating return and variance through INVF, enabling robust identification of optimal siting clusters. Subsequently, the PUO framework utilizes Markowitz Portfolio optimization that translates these siting decisions into risk-adjusted capacity allocations, highlighting the inherent trade-off between return maximization and risk mitigation according to investor risk preferences. Extending beyond the traditional Markowitz Mean-Variance framework under PUO, the Mean-CVaR portfolio optimization BESS sizing method was also applied to account for tail-risk exposure under extreme market conditions at a specified confidence level. While Mean-Variance portfolio optimization minimizes portfolio risk for a given expected return, assuming normally distributed returns. The Mean-Variance PUO model produces diversified allocations across multiple nodes, whereas increasing risk aversion leads to more concentrated investments in fewer, more stable locations, such as SME.SME_LOAD and EES.NOPLD candidate nodes that have emerged with the dominant portfolio shares of 47.4% and 45.2%, respectively. Under the Mean-CVaR PUO BESS sizing framework, the optimal capacity allocation shifts notably at SME.SME_LOAD with 38.8% allocation, followed by LAGN.LAGN with 36.6%, reflecting a more conservative distribution that prioritizes nodes with lower tail-risk exposure compared to the Mean-Variance PUO approach.

The techno-economic analysis for BESS technology selection is conducted under two base scenarios, including with and without the ITC framework, over a planning horizon from 2022 to 2037. Overall, under the "Without ITC scenario", LFP technology achieves positive NPV in 2032 and IRR in 2030, while Vd reaches profitability in 2033 under the same scenario conditions and BESS sizing frameworks. Under the "With ITC scenario", both technologies exhibit accelerated profitability, with LFP achieving positive NPV in 2030 and Vd reaching positive NPV in 2031. Overall, the highest returns were achieved by LFP technology in 2033, with an NPV of approximately USD 24.3 Million and an IRR of 18% under the With ITC scenario and Mean-CVaR PUO BESS sizing framework. The analysis incorporates realistic cost reduction trends, including a 20% year-on-year reduction in installation costs from 2020 to 2037 for the Without ITC scenario, while a 30% year-on-year reduction is applied to the Without ITC scenario costs to formulate the With ITC scenario. However, Without ITC scenario does not include $/MW components for reductions in installation cost as followed by the study. Significantly, the $/MW components associated with grid integration remain unchanged across scenarios, as they are not influenced by tax credit mechanisms. If the reductions and tax incentives were extended to these components, it may be possible that overall, BESS investment becomes feasible in earlier years. Across all scenarios, LFP consistently demonstrates better financial performance, achieving higher IRR and NPV compared to Vd, driven by its lower capital costs and well-established supply chain. However, Vd exhibits stable and resilient returns, particularly under the ITC scenario, where its longer life cycle and negligible calendar degradation contribute to sustained profitability. The sensitivity analyses applying $\pm$15% adjustments to DDL values further validate the strength of both technologies, with LFP showing greater sensitivity to revenue fluctuations in the early years, while Vd maintains steadier performance due to its degradation recovery capability.

It is worth noting that the Markowitz Portfolio optimization assumes normally distributed returns, whereas LMP data often exhibits high volatility and fat-tailed distributions, representing a general limitation of the current approach. The Mean-CVaR method inherently addresses this limitation by explicitly modeling tail risks without relying on normality assumptions, making it more suitable for electricity market applications where extreme price spikes are common. However, the clustering process identified a cluster of nodes in MISO data with approximately normal returns, thereby validating the application of Markowitz Portfolio optimization. Power grids face significant uncertainties including fuel prices, actual loads, and intermittent renewable generation profiles. However, since multi-year LMP data reflects widest possible market outcomes of grid-aware Optimal Power Flow calculations under the identified significant uncertainties, it is fair to conclude that LMPs capture most if not all uncertainties faced by the grid. Nevertheless, exclusion from any other sources of uncertainties faced by real grids is acknowledged as a limitation of the proposed research.

It is important to recognize that this study presents a preliminary framework for optimal BESS investment planning targeting private investors who lack access to detailed grid operational data. The actual BESS siting and sizing in practice requires comprehensive load flow interconnection studies, line thermal limits, voltage and phase angle constraints, transformer tap settings, contingency analysis, and detailed grid topology data all of which are typically unavailable to private investors. Despite this gap, the proposed framework still serves as a valuable data-driven decision support tool for screening potential investment opportunities under the inherent uncertainty of LMPs. By utilizing publicly available LMP signals as proxies for underlying grid conditions, the framework enables investors to make informed preliminary siting and sizing decisions before committing to join long waiting lists of costly grid interconnection studies. The ability to incorporate upper and lower bounds on portfolio shares corresponding to practical BESS size limits at selected nodes demonstrates the model's flexibility to integrate some grid constraints even without full system data access.

Looking forward, technology-specific improvements, including enhanced round-trip efficiency, increased cycle life, and extended duration capabilities, may further improve revenue streams and overall investment attractiveness. Novelty of this research lies in its robustness that it works even if grid operating conditions are not known by the investor because it leverages the potential of LMPs as signals of the underlying grid operating conditions. The proposed BESS investment approach is designed as a practical screening tool for private investors lacking grid data but their siting decisions should be coordinated with system operators. Alternatively, subscribing to services of a market or system analytics company, investors may gain limited insight into some grid operating conditions like load and renewable generation levels as well as power evacuation capacities of transmission lines connected to the local node. It is pertinent to note that already included upper and lower limits on decision variables of optimal portfolio shares, corresponding to BESS sizes at selected nodes, demonstrate inherent capability of proposed mathematical model to incorporate some grid conditions in future extensions of the research. As the BESS market continues to evolve, the proposed framework offers a scalable and adaptable tool for long-term storage investment planning in competitive electricity markets, despite limited access to grid data.

CRediT authorship contribution statement

Muhammad Umer: Writing – original draft, Visualization, Software, Methodology, Investigation, Data curation. **Kashif Imran:** Writing – original draft, Visualization, Supervision, Software, Resources, Project administration, Methodology, Investigation, Conceptualization. **Waqquas Bukhsh:** Writing – review & editing, Visualization, Software, Methodology. **Muhammad Yousif:** Writing – review & editing, Visualization, Resources, Investigation.

Declaration of competing interest

The authors declare that they have no known competing financial interests or personal relationships that could have appeared to influence the work reported in this paper.

Acknowledgements

To ensure clarity and consistency in the literature, AI language assistance (ChatGPT by OpenAI) was utilized during the editing and alignment of the results and literature review text. This support was limited to refining the language and structure of the analysis without influencing the technical content or outcomes of the study. The authors gratefully acknowledge **Mr. Ijlal Ashraf**, Director of Finance at the Sustainable Development Policy Institute (SDPI) (Email: *ijlal@sdpi.org*), for his valuable insights and guidance on the application of the Conditional Value at Risk (CVaR) method within the BESS investment planning framework. The authors also thank anonymous reviewers for their critical feedback enabling quality enhancement.

Data availability

Data will be made available on request.

References

[1] A. Goyal, K. Bhattacharya, N. Padmanabhan, LMP-based day-ahead electricity market design considering the participation of DR and BESS, in: IEEE Power and Energy Society General Meeting, IEEE Computer Society, 2022 https://doi.org/10.1109/PESGM48719.2022.9916720.

[2] A. Li, Y. Wang, L. Fan, J. Peng, Strategic Investments of Large Scale Battery Energy Storage Systems in the Wholesale Electricity Market [Online]. Available: http://arxiv.org/abs/2307.16379, Jul. 2023.

[3] G.V. Gerasimov, E.N. Gryazina, E.M. Grishin, Optimal siting and sizing of battery energy storage systems in low voltage distribution networks, in: International Conference of Young Specialists on Micro/Nanotechnologies and Electron Devices, EDM, IEEE Computer Society, 2024, pp. 1400–1403, https://doi.org/10.1109/EDM61683.2024.10615128.

[4] P.T. Kyrimlidou, C.K. Simoglou, P.N. Biskas, Optimal sizing and long-term operation of a hybrid RES-BESS station in a competitive electricity market, Sustain. Energy Grids Netw. 39 (Sep. 2024), https://doi.org/10.1016/j.segan.2024.101450.

[5] X. Fang, B.M. Hodge, L. Bai, H. Cui, F. Li, Mean-variance optimization-based energy storage scheduling considering day-ahead and real-time lmp uncertainties, IEEE Trans. Power Syst. 33 (6) (Nov. 2018) 7292–7295, https://doi.org/10.1109/TPWRS.2018.2852951.

[6] D. Krishnamurthy, C. Uckun, Z. Zhou, P.R. Thimmapuram, A. Botterud, Energy storage arbitrage under day-ahead and real-time price uncertainty, IEEE Trans. Power Syst. 33 (1) (Apr. 2017) 84–93, https://doi.org/10.1109/tpwrs.2017.2685347.

[7] Y. Zhang, P. Kou, Z. Zhang, R. Tian, Y. Yan, D. Liang, Optimal sizing and siting of BESS in high wind penetrated power systems: a strategy considering frequency and voltage control, IEEE Trans. Sustain. Energy 15 (1) (Jan. 2024) 642–657, https://doi.org/10.1109/TSTE.2023.3321302.

[8] S. Krishna, M. Deepak, R. Sunitha, Locational marginal price based scheduling strategy for effective utilization of battery energy storage in PV integrated distribution system, J. Energy Storage 94 (Jul. 2024), https://doi.org/10.1016/j.est.2024.112102.

[9] F. Fan, I. Kockar, H. Xu, J. Li, Scheduling framework using dynamic optimal power flow for battery energy storage systems, CSEE J. Power Energy Syst. 8 (1) (Jan. 2022) 271–280, https://doi.org/10.17775/CSEEJPES.2020.03710.

[10] F. Mohamad, J. Teh, C.M. Lai, Optimum allocation of battery energy storage systems for power grid enhanced with solar energy, Energy 223 (May 2021), https://doi.org/10.1016/j.energy.2021.120105.

[11] A. Muqbel, A.T. Al-Awami, M. Parvania, Optimal planning of distributed battery energy storage systems in unbalanced distribution networks, IEEE Syst. J. 16 (1) (Mar. 2022) 1194–1205, https://doi.org/10.1109/JSYST.2021.3099439.

[12] W. ur Rehman, R. Bo, H. Mehdipourpicha, J.W. Kimball, Sizing battery energy storage and PV system in an extreme fast charging station considering uncertainties and battery degradation, Appl. Energy 313 (May 2022), https://doi.org/10.1016/j.apenergy.2022.118745.

[13] W. Zhang, S. Wang, Optimal allocation of BESS in distribution network based on improved equilibrium optimizer, Front. Energy Res. 10 (2022), https://doi.org/10.3389/fenrg.2022.936592.

[14] G. Carpinelli, C. Noce, A. Russo, P. Varilone, P. Verde, Optimal siting and sizing of battery energy storage systems in unbalanced distribution systems: a multi objective problem under uncertainty, Int. J. Electr. Power Energy Syst. 162 (Nov. 2024), https://doi.org/10.1016/j.ijepes.2024.110316.

[15] G.M. Njoka, L. Mogaka, A. Wangai, Enhancing grid stability and resilience through BESS optimal placement and sizing in VRES-dominated systems, Energy Rep. 13 (Jun. 2025) 1764–1779, https://doi.org/10.1016/j.egyr.2025.01.028.

[16] D. Zhang, G.M. Shafiullah, C.K. Das, K.W. Wong, Optimal allocation of battery energy storage systems to improve system reliability and voltage and frequency stability in weak grids, Appl. Energy 377 (Jan. 2025), https://doi.org/10.1016/j.apenergy.2024.124541.

[17] Z. Zhao, Y. Shang, B. Qi, Y. Wang, Q. Zhang, Optimal sizing and siting of energy storage systems based on power grid vulnerability analysis: a trilevel optimization model, Energ. Strat. Rev. 59 (May 2025), https://doi.org/10.1016/j.esr.2025.101720.

[18] A.S. Misiç, M. Karatas, A. Dasci, Optimal sizing and location of energy storage systems for transmission grids connected to wind farms, Omega (United Kingdom) 134 (Jul. 2025), https://doi.org/10.1016/j.omega.2025.103301.

[19] K. Fida, K. Imran, K.K. Mehmood, P. Bano, A. Abusorrah, A.K. Janjua, Optimal battery energy storage system deployment from perspectives of private investors and system operators for enhancing power system reliability, J. Energy Storage 69 (Oct. 2023), https://doi.org/10.1016/j.est.2023.107882.

[20] R. Zhang, M. Lee, L. Huang, M. Ni, Optimization of battery energy storage system (BESS) sizing in different electricity market types considering BESS utilization mechanisms and ownerships, J. Clean. Prod. 470 (Sep. 2024), https://doi.org/10.1016/j.jclepro.2024.143317.

[21] A. Grimaldi, F.D. Minuto, J. Brouwer, A. Lanzini, Profitability of energy arbitrage net profit for grid-scale battery energy storage considering dynamic efficiency and

degradation using a linear, mixed-integer linear, and mixed-integer non-linear optimization approach, J. Energy Storage 95 (Aug. 2024), https://doi.org/10.1016/j.est.2024.112380.

[22] J.J. Kelly, P.G. Leahy, Optimal investment timing and sizing for battery energy storage systems, J. Energy Storage 28 (Apr. 2020), https://doi.org/10.1016/j.est.2020.101272.

[23] X. Lin, Y. Zheng, Z. Xiang, B. Wang, Optimal market-based battery energy storage system capacity sizing: considering strategic behavior of collusions in the electricity day-ahead market, J. Energy Storage 120 (Jun. 2025), https://doi.org/10.1016/j.est.2025.116309.

[24] S.S. Parvar, H. Nazaripouya, Optimal operation of battery energy storage under uncertainty using data-driven distributionally robust optimization, Electr. Power Syst. Res. 211 (Oct. 2022), https://doi.org/10.1016/j.epsr.2022.108180.

[25] K. Imran, et al., Matchmaking model for bilateral trading decisions of load serving entity, Electr. Power Syst. Res. 183 (Jun. 2020), https://doi.org/10.1016/j.epsr.2020.106281.

[26] H. Algarvio, F. Lopes, J. Sousa, J. Lagarto, Multi-agent electricity markets: retailer portfolio optimization using Markowitz theory, Electr. Power Syst. Res. 148 (Jul. 2017) 282–294, https://doi.org/10.1016/j.epsr.2017.02.031.

[27] C. Corinaldesi, D. Schwabeneder, G. Lettner, H. Auer, A rolling horizon approach for real-time trading and portfolio optimization of end-user flexibilities, Sustain. Energy Grids Netw. 24 (Dec. 2020), https://doi.org/10.1016/j.segan.2020.100392.

[28] A. Scala, A. Facchini, U. Perna, R. Basosi, Portfolio analysis and geographical allocation of renewable sources: a stochastic approach, Energy Policy 125 (Feb. 2019) 154–159, https://doi.org/10.1016/j.enpol.2018.10.034.

[29] S.B. Botero, C.M.G. Mazo, F.J.M. Arboleda, Power generation mix in Colombia including wind power: Markowitz portfolio efficient frontier analysis with machine learning, J. Open Innov.: Technol. Mark. Complex. 10 (4) (Dec. 2024), https://doi.org/10.1016/j.joitmc.2024.100402.

[30] P.A. Gbadega, Y. Sun, O.A. Balogun, Optimized energy management in grid-connected microgrids leveraging K-means clustering algorithm and artificial neural network models, Energy Convers. Manag. 336 (Jul. 2025), https://doi.org/10.1016/j.enconman.2025.119868.

[31] J.J.A. Saldanha, A. Nied, R. Trentini, R. Kutzner, AI-based optimal allocation of BESS, EV charging station and DG in distribution network for losses reduction and peak load shaving, Electr. Power Syst. Res. 234 (Sep. 2024), https://doi.org/10.1016/j.epsr.2024.110554.

[32] E. Ondigo, C. Wekesa, Economic viability of distribution network upgrade deferral through BESS sizing from K-means clustered annual load profile data, Eng. Technol. Appl. Sci. Res. 14 (3) (Jun. 2024) 14517–14524, https://doi.org/10.48084/etasr.7189.

[33] X. Wang, F. Li, Q. Zhang, Q. Shi, J. Wang, Profit-oriented BESS siting and sizing in deregulated distribution systems, IEEE Trans. Smart Grid 14 (2) (Mar. 2023) 1528–1540, https://doi.org/10.1109/TSG.2022.3150768.

[34] Market Reports, Accessed: Jul. 27, 2025[Online]. Available: https://www.misoenergy.org/markets-and-operations/real-time–market-data/market-reports/#nt=%2FMarketReportType%3AHistorical%20LMP%2FMarketReportName%3AHistorical%20Annual%20Real-Time%20LMPs%20(zip)&t=10&p=0&s=MarketReportPublished&sd=desc.

[35] P. Denholm, W. Cole, N. Blair, Moving Beyond 4-Hour Li-Ion Batteries: Challenges and Opportunities for Long(er)-Duration Energy Storage [Online]. Available: www.nrel.gov/publications, 2023.

[36] D.M. Saputra, D. Saputra, L.D. Oswari, Advances in Intelligent Systems Research, 2020.

[37] K. Mongird, V. Viswanathan, J. Alam, C. Vartanian, V. Sprenkle, R. Baxter, 2020 Grid Energy Storage Technology Cost and Performance Assessment, 2020.

[38] P. Gasper, A. Saxon, Y. Shi, E. Endler, K. Smith, F.M. Thakkar, Degradation and Modeling of Large-Format Commercial Lithium-Ion Cells as a Function of Chemistry, 1 Design, and Aging Conditions 2, 2023.

[39] K.E. Rodby, T.J. Carney, Y. Ashraf Gandomi, J.L. Barton, R.M. Darling, F. R. Brushett, Assessing the levelized cost of vanadium redox flow batteries with capacity fade and rebalancing, J. Power Sources 460 (Jun. 2020), https://doi.org/10.1016/j.jpowsour.2020.227958.

[40] Inflation Reduction Act of 2022 (H.R. 5376), Assembled by Senate and House of Representatives of the United States of America in Congress, Accessed: Mar. 28, 2026. [Online]. Available: https://www.congress.gov/117/bills/hr5376/BILLS-117hr5376enr.pdf, 2022.

[41] K. Rangelova, D. Jones, How cheap is battery storage?. https://ember-energy.org/. Accessed: Mar. 28, 2026. [Online]. Available: https://ember-energy.org/app/uploads/2025/12/How-cheap-is-battery-storage.pdf, 2025.

[42] Clean Electricity Investment Credit | Internal Revenue Service, Accessed: Mar. 28, 2026. [Online]. Available: https://www.irs.gov/credits-deductions/clean-electricity-investment-credit, 2024.

[43] A. Alizadeh, M. Esfahani, I. Kamwa, A. Moeini, S.M. Mohseni-Bonab, A useable multi-level BESSs sizing model for low-level data accessibility with risk assessment application under marketization and high uncertainties, Energy 290 (Mar. 2024), https://doi.org/10.1016/j.energy.2023.129952.

[44] A. Xuan, X. Shen, Q. Guo, H. Sun, A conditional value-at-risk based planning model for integrated energy system with energy storage and renewables, Appl. Energy 294 (Jul. 2021), https://doi.org/10.1016/j.apenergy.2021.116971.

[45] R. Khodabakhsh, S. Sirouspour, Optimal control of energy storage in a microgrid by minimizing conditional value-at-risk, IEEE Trans. Sustain. Energy 7 (3) (Jul. 2016) 1264–1273, https://doi.org/10.1109/TSTE.2016.2543024.